
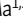
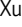

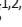
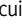
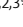
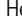
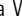


## BRIEF DEFINITIVE REPORT

# VMP1 prevents Ca<sup>2+</sup> overload in endoplasmic reticulum and maintains naive T cell survival

Ying Liu<sup>1,2\*</sup> , Yuying Ma<sup>1,2\*</sup> , Jing Xu<sup>1,2\*</sup> , Guangyue Zhang<sup>1,2,3\*</sup> , Xiaocui Zhao<sup>1,2,3\*</sup> , Zihao He<sup>1,2</sup> , Lixia Wang<sup>1,2,3</sup> ,  
Na Yin<sup>1,2</sup> , and Min Peng<sup>1,2,3,4</sup> 

Ca<sup>2+</sup> in endoplasmic reticulum (ER) dictates T cell activation, proliferation, and function via store-operated Ca<sup>2+</sup> entry. How naive T cells maintain an appropriate level of Ca<sup>2+</sup> in ER remains poorly understood. Here, we show that the ER transmembrane protein VMP1 is essential for maintaining ER Ca<sup>2+</sup> homeostasis in naive T cells. VMP1 promotes Ca<sup>2+</sup> release from ER under steady state, and its deficiency leads to ER Ca<sup>2+</sup> overload, ER stress, and secondary Ca<sup>2+</sup> overload in mitochondria, resulting in massive apoptosis of naive T cells and defective T cell response. Aspartic acid 272 (D272) of VMP1 is critical for its ER Ca<sup>2+</sup> releasing activity, and a knockin mouse strain with D272 mutated to asparagine (D272N) demonstrates all functions of VMP1 in T cells in vivo depend on its regulation of ER Ca<sup>2+</sup>. These data uncover an indispensable role of VMP1 in preventing ER Ca<sup>2+</sup> overload and maintaining naive T cell survival.

## Introduction

Ca<sup>2+</sup> is a universal and versatile second messenger in eukaryotic cells (Berridge et al., 2000). Rise of cytosolic Ca<sup>2+</sup> triggers a plethora of cellular responses such as proliferation, differentiation, contraction, secretion, cell death, and immunity (Bootman and Bultynck, 2020). ER is the major intracellular Ca<sup>2+</sup> store (Wang et al., 2019). Ca<sup>2+</sup> in ER not only supports fundamental functions of ER such as protein and lipid synthesis (Xu et al., 2005) but also plays central roles in cytosolic Ca<sup>2+</sup> signaling (Prakriya and Lewis, 2015). Upon T cell activation, TCR signaling induces ER Ca<sup>2+</sup> release through IP3R channels, and the depletion of ER Ca<sup>2+</sup> activates ER Ca<sup>2+</sup> sensor STIM1/2 that open the Ca<sup>2+</sup> release-activated channels (CRAC) on plasma membrane to induce Ca<sup>2+</sup> influx, a process called store-operated Ca<sup>2+</sup> entry (SOCE; Hogan et al., 2010). Although the critical roles of ER Ca<sup>2+</sup> depletion-induced SOCE in T cell activation, proliferation, and function are well established (Trebak and Kinet, 2019; Vaeth et al., 2020), how naive T cells maintain ER Ca<sup>2+</sup> homeostasis under steady state remains largely unexplored (Trebak and Kinet, 2019).

Ca<sup>2+</sup> in ER must be maintained at an appropriate level for proper cell function, and aberrant levels of Ca<sup>2+</sup> in ER cause ER stress and have been implicated in various diseases (Mekahli et al., 2011; Oakes and Papa, 2015; Schrank et al., 2020). Under steady state, the level of Ca<sup>2+</sup> in ER is determined by the balance of two counteracting processes that import and release Ca<sup>2+</sup>

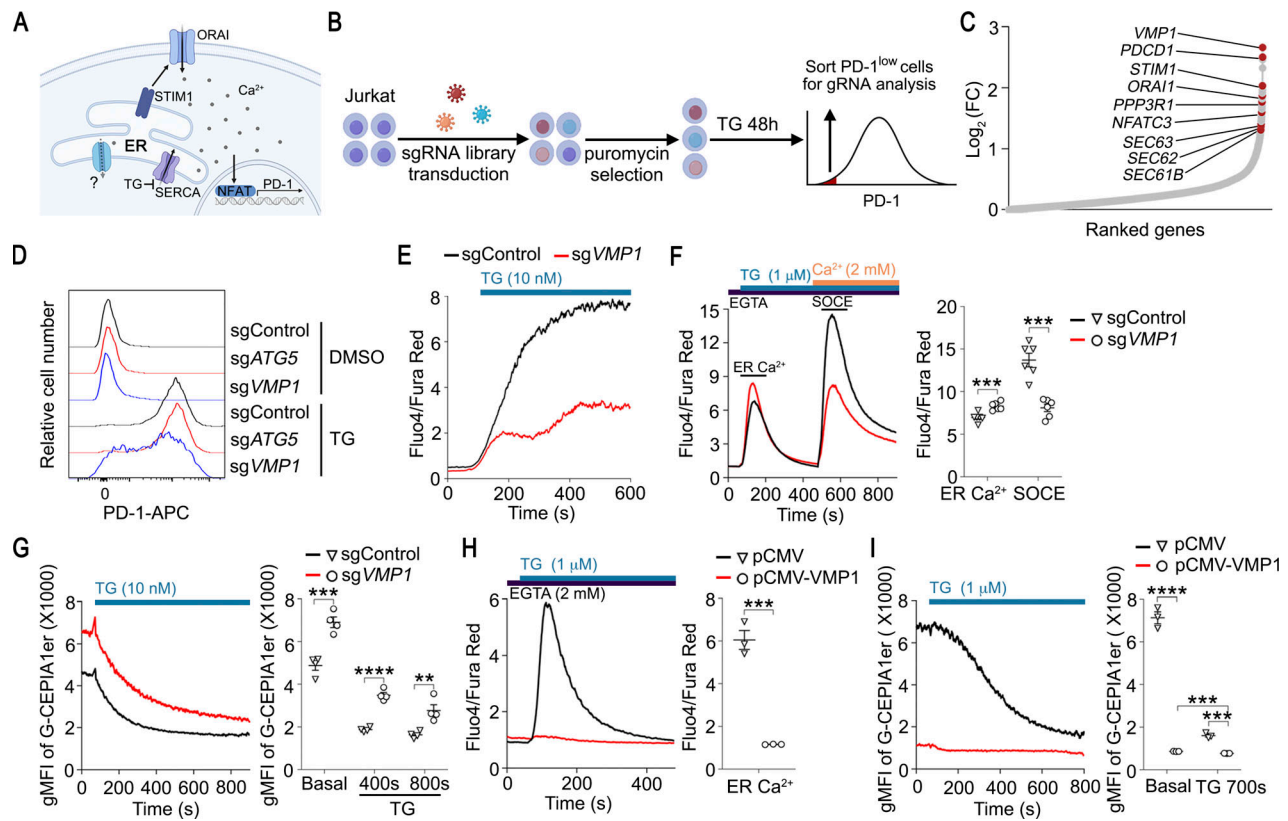
across ER membrane, respectively. The sarco/ER Ca<sup>2+</sup>-ATPases (SERCA) pump Ca<sup>2+</sup> from cytosol ([Ca<sup>2+</sup>] ~100 nM) into ER ([Ca<sup>2+</sup>] ~100 μM–1 mM) against Ca<sup>2+</sup> concentration (Wuytack et al., 2002). At the same time, ER Ca<sup>2+</sup> is passively released into cytosol under steady state to prevent ER Ca<sup>2+</sup> overload. Concentration-dependent Ca<sup>2+</sup> release from ER was documented since the 1960s (Martonosi and Feretos, 1964). Later studies showed that inhibition of SERCA by thapsigargin induces rapid drop of ER Ca<sup>2+</sup> in virtually all metazoan cells (Lewis, 2011; Thastrup et al., 1990), indicating ER Ca<sup>2+</sup> is continuously released into cytosol under steady state. How ER releases Ca<sup>2+</sup> under steady state remains incompletely understood (Camello et al., 2002; Giunti et al., 2007; Sammels et al., 2010), and its potential roles in T cell homeostasis and immunity are largely unknown (Hogan et al., 2010; Trebak and Kinet, 2019).

VMP1 is an ER-resident transmembrane protein regulating autophagy (Ropolo et al., 2007; Zhao et al., 2017), lipid metabolism (Ghanbarpour et al., 2021; Li et al., 2021; Morishita et al., 2019), and viral infections including SARS-CoV-2 (Hoffmann et al., 2021), but the molecular and physiological function of VMP1 in T cells and immunity were unknown. In this study, through genome-wide CRISPR screening for ER Ca<sup>2+</sup> regulators in T cells, we discovered that VMP1 is indispensable for protection of ER and mitochondrion from Ca<sup>2+</sup> overload, which maintains naive T cell survival and T cell immunity.

<sup>1</sup>Department of Basic Medical Sciences, School of Medicine, Tsinghua University, Beijing, China; <sup>2</sup>Institute for Immunology, Tsinghua University, Beijing, China; <sup>3</sup>Tsinghua-Peking Center for Life Sciences, Beijing, China; <sup>4</sup>Beijing Key Laboratory for Immunological Research on Chronic Diseases, Tsinghua University, Beijing, China.

\*Y. Liu, Y. Ma, J. Xu, G. Zhang, and X. Zhao contributed equally to this paper. Correspondence to Min Peng: pengmin@tsinghua.edu.cn.

© 2023 Liu et al. This article is distributed under the terms of an Attribution–Noncommercial–Share Alike–No Mirror Sites license for the first six months after the publication date (see <http://www.rupress.org/terms/>). After six months it is available under a Creative Commons License (Attribution–Noncommercial–Share Alike 4.0 International license, as described at <https://creativecommons.org/licenses/by-nc-sa/4.0/>).



**Figure 1. Genome-wide CRISPR screening reveals VMP1 promotes ER Ca<sup>2+</sup> release.** (A) A cartoon illustrating SOCE and thapsigargin (TG)-Ca<sup>2+</sup>-NFAT-PD-1 signaling axis. (B) CRISPR screening strategy. (C) Screening result from Jurkat cells. Selected top hits are labeled. (D) Jurkat cells expressing indicated sgRNAs and Cas9 were treated with DMSO or TG (10 nM) for 48 h, and the expression of PD-1 was examined by flow cytometry. Mean fluorescence intensities of PD-1 staining are shown. (E) TG-induced SOCE in Jurkat cells expressing indicated sgRNAs and Cas9 was examined by flow cytometry. (F) ER Ca<sup>2+</sup> and SOCE in HEK293T cells expressing indicated sgRNAs and Cas9 were examined by flow cytometry. (G) ER Ca<sup>2+</sup> before and after TG (10 nM) treatment was monitored by flow cytometry. (H) HEK293T cells were transfected with indicated plasmids together with a BFP reporter. ER Ca<sup>2+</sup> of BFP<sup>high</sup> cells was examined by flow cytometry. (I) HEK293T-G-CePIA1er cells were transfected with indicated plasmids together with a BFP reporter. Fluorescence intensity of G-CePIA1er in BFP<sup>high</sup> cells before and after TG (1 μM) treatment was measured by flow cytometry. (D and E) Representative plots from one of three independent experiments. (F–I) Representative plots and statistics from one of three independent experiments; *n* = 6 in F, *n* = 4 in G, *n* = 3 in H and I. Each symbol represents one sample; data represent mean ± SEM, two-tailed unpaired *t* test in F and H, two-way ANOVA in G and I, \*\*\* <0.01, \*\*\*\* <0.001, \*\*\*\*\* <0.0001.

## Results and discussion

### Genome-wide CRISPR screening reveals VMP1 is required for SOCE

To identify protein(s) involved in ER Ca<sup>2+</sup> release in T cells, we performed genome-wide CRISPR screening with Ca<sup>2+</sup>-NFAT-PD-1 signaling axis as the readout (Fig. 1 A). SOCE is required for T cell activation and upregulation of surface proteins including PD-1 via NFAT (Oestreich et al., 2008; Trebak and Kinet, 2019; Vaeth et al., 2020). The rationale of our screening was that T cells devoid of a putative protein required for ER Ca<sup>2+</sup> release would have increased basal level of ER Ca<sup>2+</sup>, which would be partially resistant to thapsigargin-induced SOCE, resulting in reduced PD-1 upregulation.

Thapsigargin treatment induced robust SOCE in human Jurkat T cells (Fig. S1 A), which upregulated PD-1 in an NFAT-dependent manner, as indicated by its inhibition by the NFAT inhibitor cyclosporine A (Fig. S1 B). Thapsigargin is an irreversible inhibitor of SERCA, which causes persistent ER Ca<sup>2+</sup> depletion, ER stress, and cell death (Lewis, 2011; Thastrup et al., 1990). We titrated thapsigargin to balance PD-1 induction and toxicity and found that

10 nM of thapsigargin treatment for 48 h potently induced PD-1 expression in Jurkat cells with minimal toxicity (Fig. S1, C and D).

Then, we performed genome-wide CRISPR screening in Jurkat cells for genes whose loss-of-function resulted in blunted upregulation of PD-1 upon thapsigargin treatment (Fig. 1 B and Table S1). As expected, PD-1 itself and NFAT pathway components (NFATc3 and PPP3R1) were among the top hits (Fig. 1 C and Table S1). In addition, SOCE components STIM1 and ORAI1 were among the top hits (Fig. 1 C and Table S1). Translocon components (SEC61, SEC62, and SEC63) were also among the top hits (Fig. 1 C and Table S1), in agreement with passive leak of small molecules including Ca<sup>2+</sup> by translocon (Giunti et al., 2007; Lomax et al., 2002; Roy and Wonderlin, 2003). The recovery of key players of SOCE (STIM1/ORAI1), NFAT signaling (NFATc3 and PPP3R1), and ER Ca<sup>2+</sup> release (SEC61/SEC62/SEC63) as top hits demonstrates that our screening strategy is feasible. Unexpectedly, VMP1, an ER transmembrane protein without known roles in PD-1 regulation, was the top hit of our PD-1-based screening (Fig. 1 C and Table S1).

We validated that thapsigargin-induced upregulation of PD-1 was blunted in VMP1-deficient Jurkat cells (Fig. 1 D and Fig. S1 E). Previous studies showed that VMP1 regulates autophagy (Ropolo et al., 2007; Zhao et al., 2017). We found that ATG5, a protein essential for autophagy, did not regulate thapsigargin-induced PD-1 upregulation (Fig. 1 D), which is consistent with our screening data that canonical autophagy genes were not hits in our screening (Table S1).

To test whether VMP1 regulates SOCE, we monitored cytosolic  $\text{Ca}^{2+}$  rise in response to thapsigargin treatment and found that SOCE was inhibited in VMP1-deficient Jurkat T cells (Fig. 1 E and Fig. S1 E). ATG5 did not regulate thapsigargin-induced  $\text{Ca}^{2+}$  influx (Fig. S1 F). These data demonstrate that VMP1 regulates PD-1 expression and SOCE independent of autophagy.

Together, using  $\text{Ca}^{2+}$ -NFAT-PD-1 signaling as the readout for genome-wide CRISPR screening of ER  $\text{Ca}^{2+}$  regulators, we identified VMP1 as a novel regulator of SOCE in Jurkat T cells.

### VMP1 deficiency causes ER $\text{Ca}^{2+}$ overload while overexpression of VMP1 depletes ER $\text{Ca}^{2+}$

SOCE is functional in almost all metazoan cells (Lewis, 2011). So, we examined whether VMP1 regulates SOCE in other cell types. To separate thapsigargin-releasable  $\text{Ca}^{2+}$  (mostly from ER, hereafter referred to as ER  $\text{Ca}^{2+}$ ) and  $\text{Ca}^{2+}$  influx from outside of cells (SOCE),  $\text{Ca}^{2+}$  in assay medium (DMEM, which contains 1.8 mM  $\text{Ca}^{2+}$ ) was chelated by 2 mM EGTA before thapsigargin treatment and then 2 mM  $\text{Ca}^{2+}$  was added back to induce  $\text{Ca}^{2+}$  influx (Bird et al., 2008). Using this classic SOCE protocol, we found that VMP1 deficiency increased ER  $\text{Ca}^{2+}$  and inhibited SOCE in HEK293T cells (Fig. 1 F and Fig. S1 G). The above results were obtained in polyclonal KO cells (Fig. S1 G), which were validated in multiple monoclonal VMP1 KO cell lines (Fig. S1, H and I).

To monitor ER  $\text{Ca}^{2+}$  directly, we established HEK293T cells stably expressing an ER-targeted  $\text{Ca}^{2+}$  sensor G-CEPIA1er (Suzuki et al., 2014), named HEK293T-G-CEPIA1er, whose green fluorescence reflects ER  $\text{Ca}^{2+}$  level. Flow cytometry-based measurement of G-CEPIA1er intensity showed that ER  $\text{Ca}^{2+}$  was increased in the absence of VMP1, both under steady state and after thapsigargin treatment (Fig. 1 G and Fig. S1 J). These data provide direct evidence that VMP1 deficiency increases ER  $\text{Ca}^{2+}$  store, but the increased ER  $\text{Ca}^{2+}$  can still be slowly released via other mechanisms, likely via translocon (Giunti et al., 2007; Lomax et al., 2002; Roy and Wonderlin, 2003).

To test whether VMP1 promotes ER  $\text{Ca}^{2+}$  release, we overexpressed VMP1 in HEK293T cells. ER  $\text{Ca}^{2+}$  was almost completely depleted in cells overexpressing VMP1 (Fig. 1 H), indicating most ER  $\text{Ca}^{2+}$  was depleted by VMP1 overexpression. Consistently, in HEK293T-G-CEPIA1er cells, overexpression of VMP1 almost completely depleted ER  $\text{Ca}^{2+}$  under steady state, and minimal ER  $\text{Ca}^{2+}$  release was observed after thapsigargin treatment (Fig. 1 I). These data demonstrate that VMP1 promotes ER  $\text{Ca}^{2+}$  release in HEK293T cells, directly or indirectly.

### Plasma membrane-targeted VMP1 induces $\text{Ca}^{2+}$ influx

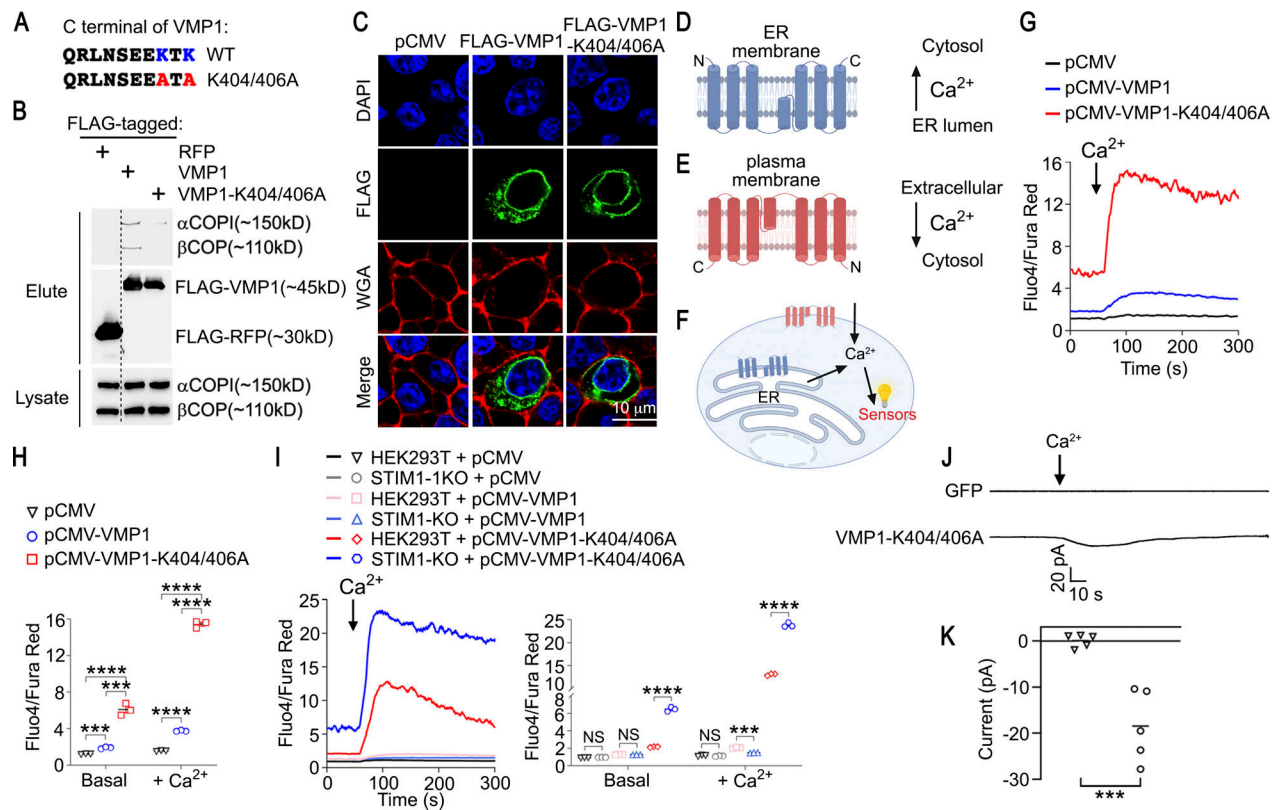
VMP1 is an ER-resident membrane protein (Tábara and Escalante, 2016; Zhao et al., 2017). It is difficult to monitor

$\text{Ca}^{2+}$  transport across ER membrane, so we tried to redirect VMP1 to plasma membrane where  $\text{Ca}^{2+}$  influx can be easily monitored. VMP1 has a di-lysine-based Golgi-to-ER retrieve motif at their C-terminals (Fig. 2 A; Arakel and Schwappach, 2018). This motif interacts with the COPI complex that retro-transport membrane proteins from trans-Golgi back to ER, a process critical for correct localization of membrane proteins (Arakel and Schwappach, 2018). When lysine residues within the Golgi-to-ER retrieve motif of VMP1 were mutated to alanine, the resulting VMP1-K404/406A mutant showed reduced COPI binding compared with their WT counterparts (Fig. 2 B). Unlike WT VMP1 showing typical ER localization as reported previously (Tábara and Escalante, 2016; Zhao et al., 2017; Fig. 2 C), VMP1-K404/406A showed plasma membrane localization in addition to ER (Fig. 2 C).

According to membrane protein topology, the lumen side of VMP1 should face extracellularly when these proteins are expressed on plasma membrane (Fig. 2, D and E). The direction of ion flow depends on electrochemical gradient of ions across membrane (Alberts et al., 2002). Since  $\text{Ca}^{2+}$  concentrations are high in ER and extracellular space ( $\sim$  mM range) and very low in cytosol ( $\sim$  nM range), plasma membrane-targeted VMP1-K404/406A should cause  $\text{Ca}^{2+}$  influx if they are able to promote  $\text{Ca}^{2+}$  transport (Fig. 2 F). We used two independent methods to monitor  $\text{Ca}^{2+}$  influx, the fluorescent  $\text{Ca}^{2+}$  sensor RCaMP1h expressed in cytosol (Akerboom et al., 2013), and the  $\text{Ca}^{2+}$  indicators Fluo4/Fura Red. In both assays, supplementation of  $\text{Ca}^{2+}$  to empty vector-transfected HEK293T cells induced neglectable  $\text{Ca}^{2+}$  influx (Fig. 2, G and H; and Fig. S2 A). This result is consistent with the fact that most cells do not express concentration-dependent  $\text{Ca}^{2+}$  channels on cell surface, and all  $\text{Ca}^{2+}$  channels on plasma membrane are tightly gated by certain mechanisms (Owsianik et al., 2006). In cells overexpressing WT VMP1, supplementation of  $\text{Ca}^{2+}$  induced a small  $\text{Ca}^{2+}$  influx while a robust  $\text{Ca}^{2+}$  influx was detected in cells overexpressing the plasma membrane-targeted VMP1-K404/406A (Fig. 2, G and H; and Fig. S2 A). Moreover,  $\text{Ca}^{2+}$  influx in cells overexpressing VMP1-K404/406A was concentration dependent (Fig. S2 B).

To explore whether plasma membrane-targeted VMP1-K404/406A induces  $\text{Ca}^{2+}$  influx via SOCE, we used STIM1 KO cells and CRAC channel inhibitor CM4620, both abolishing SOCE (Fig. S2, C-E). The small  $\text{Ca}^{2+}$  influx induced by WT VMP1 was completely inhibited by STIM1 deficiency or CM4620 (Fig. 2 I and Fig. S2 F), demonstrating their SOCE nature. Surprisingly,  $\text{Ca}^{2+}$  influx induced by VMP1-K404/406A was not inhibited, but, in fact, was enhanced by STIM1 deficiency or CM4620 (Fig. 2 I and Fig. S2 F), demonstrating that  $\text{Ca}^{2+}$  influx induced by plasma membrane-targeted VMP1 is unlikely to be SOCE. These data also suggest that STIM1/ORAI1 may influence the activity of VMP1.

ORAI1 is the pore component of CRAC (Hogan et al., 2010), which was required for SOCE in HEK293T cells (Fig. S2 G). However, ORAI1 was not required for VMP1-K404/406A-mediated  $\text{Ca}^{2+}$  influx (Fig. S2 H), suggesting that VMP1-K404/406A-mediated  $\text{Ca}^{2+}$  influx is unlikely to be SOCE. To test whether VMP1-K404/406A induced  $\text{Ca}^{2+}$  influx by opening other  $\text{Ca}^{2+}$  channels, we screened a library of 652 compounds targeting known ion channels/membrane transporters, including



**Figure 2. VMP1 promotes Ca<sup>2+</sup> transport across membranes.** (A) C-terminal amino acid sequence of VMP1. Lysine residues in the Golgi-to-ER retrieve motif are labeled in blue and the mutated alanine was labeled in red. (B) The interactions between RFP, VMP1, or VMP1-K404/406A with COPI were examined by coimmunoprecipitation. Irrelevant lanes were removed and a dash line is shown. (C) Subcellular localization of FLAG-tagged (N-terminal) VMP1 and VMP1-K404/406A was examined by immunofluorescence. Plasma membrane was labeled by WGA. (D) Putative topology of VMP1 on ER. (E) Putative topology of VMP1-K404/406A on plasma membrane. (F) An illustration of Ca<sup>2+</sup> transport mediated by VMP1 on ER and VMP1-K404/406A on plasma membrane. (G and H) Ca<sup>2+</sup> influx in HEK293T cells transfected with empty vector, VMP1, or VMP1-K404/406A was measured by flow cytometry with 8 mM CaCl<sub>2</sub>. (I) Ca<sup>2+</sup> influx in HEK293T or STIM1-KO HEK293T cells transfected with empty vector, VMP1, or VMP1-K404/406A was measured by flow cytometry with 8 mM CaCl<sub>2</sub>. (J and K) Whole-cell patch-clamp traces of STIM1-KO HEK293T cells transfected with pCMV-GFP or pCMV-VMP1-K404/406A. Final concentration of 20 mM CaCl<sub>2</sub> was added to bath solution. The holding potential was -100 mV. (B and C) Representative data from one of three independent experiments. (G–I) Representative plots and statistics from one of three independent experiments. (J and K) Representative plots and statistics from one of five independent experiments; *n* = 3 in H and I, *n* = 5 in K. Each symbol represents one sample; data represent mean ± SEM, two-way ANOVA in H and I, two-tailed unpaired *t* test in K; \*\*\* < 0.001, \*\*\*\* < 0.0001. Source data are available for this figure: SourceData F2.

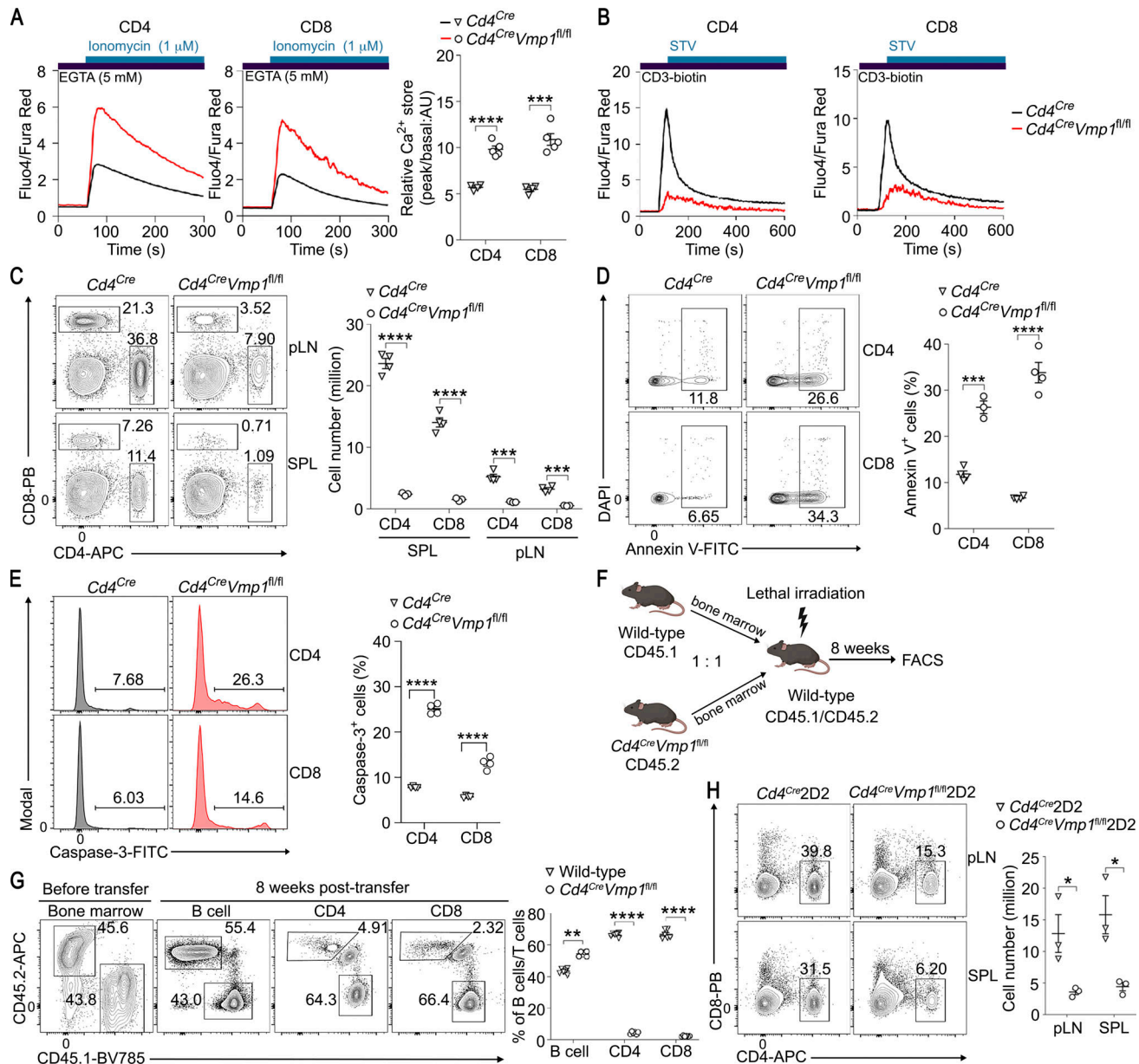
all Ca<sup>2+</sup> channels in HEK293T-RCaMP1h cells transfected with VMP1-K404/406A (Fig. S2 I). Potent inhibition of SOCE by the CRAC channel inhibitor CM4620 from this library was validated (Fig. S2 E). No compound from this library was able to inhibit Ca<sup>2+</sup> influx induced by VMP1-K404/406A (Fig. S2 J). As a control, the Ca<sup>2+</sup> chelator EGTA prevented Ca<sup>2+</sup> influx induced by VMP1-K404/406A (Fig. S2 J).

We performed whole-cell patch-clamp experiments to investigate the electrophysiology of VMP1-K404/406A. STIM1-deficient HEK293T cells were used in these experiments for two reasons: (1) VMP1-K404/406A-mediated Ca<sup>2+</sup> influx was stronger in STIM1-deficient cells (Fig. 2 I) and (2) SOCE was absent in these cells (Fig. S2, C and D). We recorded a weak but consistent inward current in STIM1-deficient cells expressing VMP1-K404/406A after supplementation of Ca<sup>2+</sup> extracellularly (Fig. 2, J and K). Taken together, these data demonstrate that VMP1 promotes Ca<sup>2+</sup> transport across membrane, directly or indirectly. Whether VMP1 is a Ca<sup>2+</sup> channel or not warrants further investigations.

### VMP1 deficiency results in ER Ca<sup>2+</sup> overload and naive T cell apoptosis

Germline-KO of *Vmp1* in mice leads to early embryonic lethality due to unknown reason(s) (Calvo-Garrido et al., 2008; Morishita et al., 2019). We generated a conditional allele of *Vmp1* (Fig. S3 A) and specifically deleted this gene in T cells with *Cd4<sup>Cre</sup>* (Fig. S3 B).

We used the Ca<sup>2+</sup> ionophore ionomycin (1 μM) to measure ER Ca<sup>2+</sup> stored in primary mouse T cells. When extracellular Ca<sup>2+</sup> is chelated with EGTA, the rise of cytosolic Ca<sup>2+</sup> upon ionomycin treatment indicates the intracellular Ca<sup>2+</sup> store, mainly from ER (Bird et al., 2008). Under steady state, ER Ca<sup>2+</sup> store was significantly increased in T cells from *Cd4<sup>Cre</sup>Vmp1<sup>f/f</sup>* mice compared with that from control mice (Fig. 3 A), which is consistent with increased ER Ca<sup>2+</sup> in VMP1-deficient HEK293T cells (Fig. 1, F and G), demonstrating that VMP1 deficiency causes ER Ca<sup>2+</sup> overload in different cell types. CD3ε crosslinking induced Ca<sup>2+</sup> influx was reduced in VMP1-deficient T cells compared with WT cells (Fig. 3 B), which is in line with reduced SOCE in VMP1-



**Figure 3. VMP1 deficiency results in ER Ca<sup>2+</sup> overload and naive T cell apoptosis.** (A) ER Ca<sup>2+</sup> stored in T cells from mice with indicated genotypes was examined by flow cytometry. Representative plots and statistics are shown. (B) Ca<sup>2+</sup> influx triggered by CD3ε crosslinking in T cells from mice with indicated genotypes was examined by flow cytometry. T cells were incubated with 10 μg/ml anti-CD3-biotin, then 10 μg/ml streptavidin (STV) was used for cross-linking. (C) Absolute number of T cells from spleen (SPL) and peripheral lymph nodes (pLN) of mice with indicated genotypes. Mice were 4–6 wk old. (D) Apoptosis of freshly isolated T cells from mice with indicated genotypes was analyzed by flow cytometry. (E) Caspase-3 staining of freshly isolated T cells from mice with indicated genotypes was analyzed by flow cytometry. (F) Experimental setup for BM chimera experiments. (G) Flow cytometry analysis of donor-derived cells before transfer and 8 wk after transfer. (H) Cells from SPL and pLN of mice with indicated genotypes were analyzed by flow cytometry. (A, C–E, G, and H) Representative plots and statistics from one of two independent experiments. (B) Representative plots from one of three independent experiments. *n* = 5 mice per genotype in A, *n* = 3–4 mice per genotype in C, *n* = 4 mice per genotype in D and E, *n* = 6 mice per genotype in G, *n* = 3 mice per genotype in H; each symbol represents an individual mouse; data represent mean ± SEM, two-tailed unpaired *t* test; \* < 0.05, \*\* < 0.01, \*\*\* < 0.001, \*\*\*\* < 0.0001.

deficient Jurkat T cells (Fig. 1 E). These data suggest that insufficient depletion of ER Ca<sup>2+</sup> in VMP1-deficient cells partially blocks SOCE.

Deletion of *Vmp1* with *Cd4*<sup>Cre</sup> did not affect T cell development in thymus (Fig. S3 C). However, there was a drastic reduction of T cell number in secondary lymphoid organs of *Cd4*<sup>Cre</sup>*Vmp1*<sup>fl/fl</sup> mice compared with those of control mice (Fig. 3 C), which is

associated with increased apoptosis of VMP1-deficient T cells (Fig. 3, D and E; and Fig. S3 D). Consistent with dramatic reduction of peripheral T cells, *Cd4*<sup>Cre</sup>*Vmp1*<sup>fl/fl</sup> mice were unable to mount an antigen-specific T cell response to *Listeria monocytogenes* infection (Fig. S3, E and F).

To exclude cell-extrinsic effects of *Cd4*<sup>Cre</sup>*Vmp1*<sup>fl/fl</sup> mice, we performed bone marrow (BM) chimera experiments. BM cells

from congenically marked control mice (CD45.1/45.1) and *Cd4<sup>Cre</sup>Vmp1<sup>fl/fl</sup>* mice (CD45.2/45.2) were mixed at a 1:1 ratio and transferred into lethally irradiated recipient mice (CD45.1/45.2; Fig. 3 F). After 8 wk, there were 10–20-fold more T cells derived from BM of control mice than that from *Cd4<sup>Cre</sup>Vmp1<sup>fl/fl</sup>* mice, while the reconstitution of B cells was not affected (Fig. 3 G), demonstrating that the survival defect of VMP1-deficient T cells is cell-intrinsic.

To exclude the potential influence of TCR repertoire on the phenotype of VMP1-deficient mice, we bred *Cd4<sup>Cre</sup>Vmp1<sup>fl/fl</sup>* mice to the 2D2 transgenic mice expressing a myelin oligodendrocyte glycoprotein-specific TCR. When TCR was fixed to 2D2, there was still pronounced reduction of peripheral T cells in *Cd4<sup>Cre</sup>Vmp1<sup>fl/fl</sup>2D2* mice compared with those from control 2D2 mice (Fig. 3 H), demonstrating that the survival defect of VMP1-deficient T cells is not due to potential differences of TCR repertoire between control and VMP1-deficient mice.

Together, these data demonstrate that VMP1 deficiency results in ER Ca<sup>2+</sup> overload in T cells under steady state, which causes dramatic reduction of peripheral T cells that is associated with increased apoptosis of these cells.

#### All functions of VMP1 in T cells depend on its regulation of ER Ca<sup>2+</sup>

We then explored whether increased apoptosis of VMP1-deficient T cells is caused by ER Ca<sup>2+</sup> overload. The selectivity of Ca<sup>2+</sup> transport is usually determined by several negatively charged amino acids that form a glutamate or aspartate ring near the pore region (Owsianik et al., 2006). To identify such key amino acids in VMP1, we established a rescue system where VMP1 and mutants were re-expressed in VMP1-deficient cells at relatively physiological level. We used a lentiviral vector that expresses protein at a level lower than that of pCMV vector, which we used in overexpression experiments (Fig. S3, G and H), and only mildly depleted ER Ca<sup>2+</sup> was detected from this VMP1 expressed cell (Fig. S3 I).

There are five negatively charged amino acids in VMP1 that are both close to a transmembrane segment and face the ER lumen side (Fig. 4 A). Mutation of aspartic acid 272 (D272) to asparagine (D272N) completely abolished VMP1's ability to decrease ER Ca<sup>2+</sup> and restore SOCE in VMP1-deficient cells, while all other mutants behaved as WT VMP1 (Fig. 4, B and C). We observed the autophagy defect of VMP1-deficient HEK293T cells, judged by p62 accumulation and LC3 lipidation, was rescued by WT VMP1, but not by VMP1-D272N (Fig. S3 J), demonstrating that regulation of autophagy by VMP1 in HEK293T cells requires its regulation of ER Ca<sup>2+</sup>.

We then generated a VMP1-D272N knockin mouse strain (*Vmp1<sup>D272N/+</sup>*; Fig. S3, K–M). Heterozygous *Vmp1<sup>D272N/+</sup>* mice developed normally (data not shown) and did not show changes in ER Ca<sup>2+</sup> level (Fig. S3 N), indicating VMP1-D272N did not function as a dominant-negative mutant to interfere with the function of WT VMP1 protein. However, homozygous *Vmp1<sup>D272N/D272N</sup>* mice could not be obtained from heterozygous intercrossing (data not shown), suggesting embryonic lethality of *Vmp1<sup>D272N/D272N</sup>* mice, a reminiscence of *Vmp1* germline-KO mice (Calvo-Garrido et al., 2008).

We generated *Cd4<sup>Cre</sup>Vmp1<sup>fl/D272N</sup>* mice with one allele of *Vmp1* encoding VMP1-D272N and the other was *Vmp1*-null, in which only the mutant VMP1-D272N proteins were expressed in T cells. T cells from *Cd4<sup>Cre</sup>Vmp1<sup>fl/D272N</sup>* mice had the identical ER Ca<sup>2+</sup> overload and survival defect as those from *Cd4<sup>Cre</sup>Vmp1<sup>fl/fl</sup>* mice (Fig. 4, D and E), demonstrating that D272 is absolutely required for VMP1 to regulate ER Ca<sup>2+</sup> release and mutation of this key amino acid completely abolishes VMP1's physiological function in T cells in vivo.

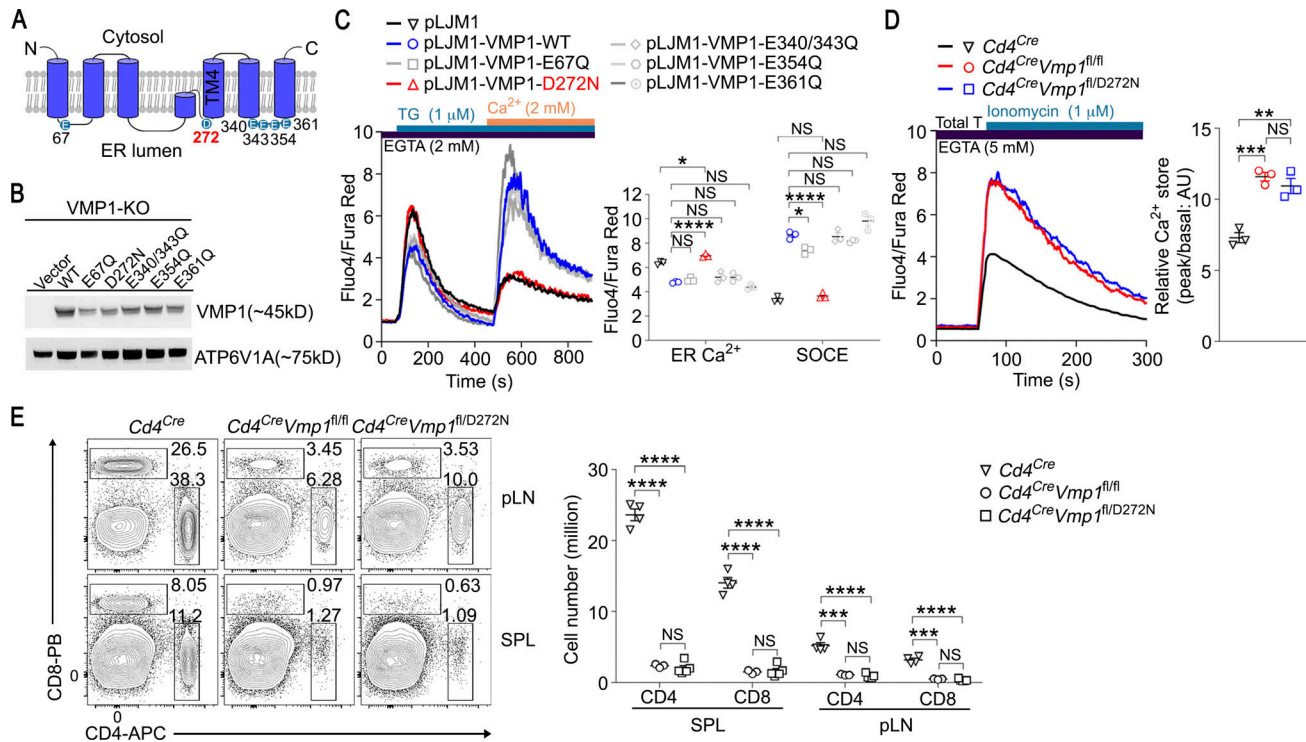
Together, by identification of the key amino acid of VMP1 required for ER Ca<sup>2+</sup> release and generation of a knockin mice strain, we demonstrate that all functions of VMP1 in T cells depend on its regulation of ER Ca<sup>2+</sup> in vivo.

#### ER and mitochondrial Ca<sup>2+</sup> overload cause apoptosis of VMP1-deficient T cells

We then examined the downstream events of ER Ca<sup>2+</sup> overload in VMP1-deficient T cells. The activity of ER chaperons responsible for protein folding is regulated by luminal Ca<sup>2+</sup> (Xu et al., 2005). Changes in ER Ca<sup>2+</sup> level affect protein synthesis and induce unfolded protein response (UPR) and ER stress (Xu et al., 2005). Indeed, we found phosphorylation of eIF2 $\alpha$  at serine 51 (peIF2 $\alpha$ -S51), a well-established marker of ER stress, was significantly increased in freshly isolated T cells from *Cd4<sup>Cre</sup>Vmp1<sup>fl/fl</sup>* mice compared with those from control mice (Fig. 5 A), demonstrating that VMP1-deficient T cells undergo constitutive ER stress under steady state. Importantly, no difference in peIF2 $\alpha$ -S51 was observed in T cells from *Cd4<sup>Cre</sup>Vmp1<sup>fl/fl</sup>* and *Cd4<sup>Cre</sup>Vmp1<sup>fl/D272N</sup>* mice (Fig. 5 A), demonstrating that ER stress is directly associated with VMP1's ability to regulate ER Ca<sup>2+</sup> release. Similarly, ER stress in VMP1-deficient HEK293T cells was rescued by WT VMP1, but not by VMP1-D272N (Fig. S3 J), demonstrating that regulation of ER Ca<sup>2+</sup> by VMP1 prevents ER stress in different cell types. Among three branches of UPR (Xu et al., 2005), only activation of eIF2 $\alpha$  was observed in VMP1-deficient T cells while the activation of ATF6 and IRE1 branches of UPR was not detected (data not shown), suggesting ER stress in VMP1-deficient T cells is likely mild and there might be additional consequence of ER Ca<sup>2+</sup> overload that contributes to the apoptosis of these cells.

It is known that mitochondria take up Ca<sup>2+</sup> from ER via the mitochondrion–ER contact sites called mitochondria-associated membrane (Patergnani et al., 2011), and mitochondrial Ca<sup>2+</sup> overload is known to trigger cell death (Giorgi et al., 2012). We hypothesized that Ca<sup>2+</sup> overload in ER might cause overflow of Ca<sup>2+</sup> into mitochondria. Thus, we examined the influence of VMP1 deficiency on mitochondrial Ca<sup>2+</sup> with the mitochondria-specific Ca<sup>2+</sup> dye Rhod2. To exclude the influence of growth factors and extracellular Ca<sup>2+</sup> on the measurement of mitochondrial Ca<sup>2+</sup> (Patergnani et al., 2011), we used serum-free RPMI 1640 with 5 mM EGTA as assay buffer. Compared with those from control mice, T cells from both *Cd4<sup>Cre</sup>Vmp1<sup>fl/fl</sup>* and *Cd4<sup>Cre</sup>Vmp1<sup>fl/D272N</sup>* mice showed increased levels of mitochondrial Ca<sup>2+</sup> (Fig. 5 B).

To explore whether mitochondrial Ca<sup>2+</sup> overload is secondary to ER Ca<sup>2+</sup> overload, we tried to use thapsigargin, which depletes ER Ca<sup>2+</sup> (Lewis, 2011; Thastrup et al., 1990), to relieve mitochondrial



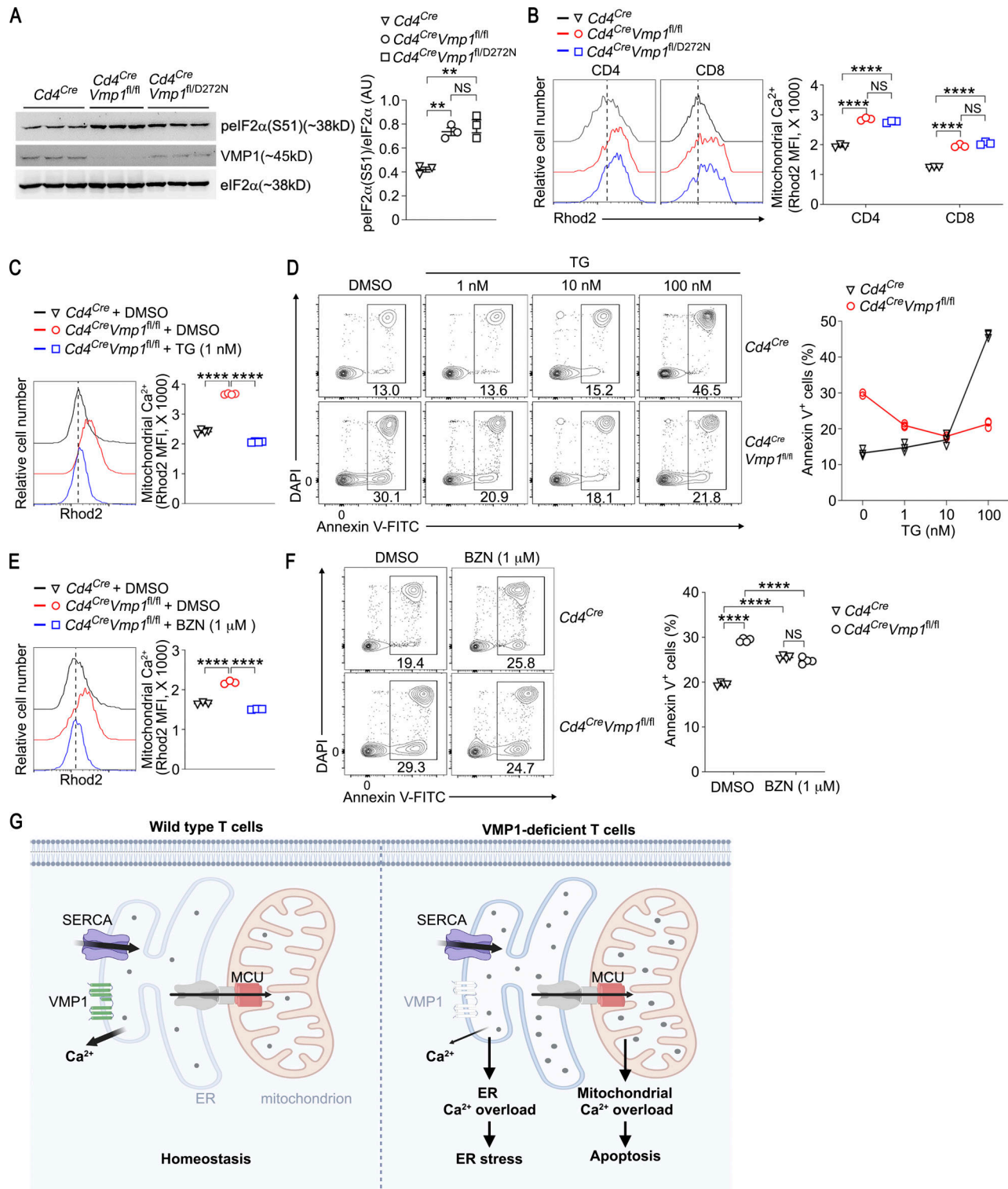
**Figure 4. Aspartic acid 272 of VMP1 is critical for its regulation of ER Ca<sup>2+</sup> release and naive T cell survival.** (A) Putative topology of VMP1 protein. Negatively charged amino acids on the ER lumen side that are also close to a transmembrane segment are indicated, including E67, D272, E340/343, E354, and E361. (B) VMP1-KO HEK293T cells were transfected with indicated plasmids. The expression of VMP1 and mutants was examined by immunoblot. (C) VMP1-KO HEK293T cells were transfected with indicated plasmids. ER Ca<sup>2+</sup> and SOCE were measured by flow cytometry. (D) ER Ca<sup>2+</sup> stored in T cells from mice with indicated genotypes was examined by flow cytometry. (E) Representative flow cytometry plots and absolute number of T cells in spleen (SPL) and peripheral lymph nodes (pLN) from mice with indicated genotypes. Mice were 4–6 wk old. T cell number of *Cd4<sup>Cre</sup>* and *Cd4<sup>Cre</sup>Vmp1<sup>fl/fl</sup>* mice were from the same mice in Fig. 3 C. (B) Representative blots from one of two independent experiments. (C) Representative plots and statistics from one of three independent experiments. (D and E) Representative plots and statistics from one of two independent experiments. *n* = 3 in C, *n* = 3 mice per genotype in D, *n* = 3–4 mice per genotype in E; each symbol represents one sample or an individual mouse; data represent mean ± SEM, two-way ANOVA in C, one-way ANOVA in D and E; \* <0.05, \*\* <0.01, \*\*\* <0.001, \*\*\*\* <0.001. Source data are available for this figure: SourceData F4.

Ca<sup>2+</sup> overload in VMP1-deficient T cells. Thapsigargin induced robust SOCE in T cells (Fig. S1 A), resulting in partial activation of T cells (data not shown). Thus, we used RPMI 1640 with 5 mM EGTA as assay buffer to prevent SOCE. We found that the increase of mitochondrial Ca<sup>2+</sup> in VMP1-deficient T cells was reversed by thapsigargin treatment (Fig. 5 C), demonstrating that mitochondrial Ca<sup>2+</sup> overload in VMP1-deficient T cells is secondary to ER Ca<sup>2+</sup> overload.

We then examined the effect of thapsigargin on apoptosis of control and VMP1-deficient T cells. Similar to our observation in Jurkat cells (Fig. S1 D), thapsigargin treatment induced cell death in a dose-dependent manner in primary T cells (Fig. 5 D), which is consistent with the fact that thapsigargin, an irreversible inhibitor of SERCA, causes persistent ER Ca<sup>2+</sup> depletion and cell death (Lewis, 2011; Thastrup et al., 1990). For VMP1-deficient T cells (Fig. 5 E; De Mario et al., 2021). Importantly, although BZN was toxic to control T cells, it largely reversed the apoptosis of VMP1-deficient T cells (Fig. 5 F), demonstrating mitochondrial Ca<sup>2+</sup> overload causes apoptosis of VMP1-deficient T cells. Finally, we tried to rescue T cell number in *Cd4<sup>Cre</sup>Vmp1<sup>fl/fl</sup>* mice with daily injection of BZN for 4 wk. However, no rescue of T cell number was observed (data not shown). Multiple limitations could explain the failure of in vivo rescue experiments with BZN, including drug dose, duration, and toxicity of BZN itself

of Ca<sup>2+</sup> in ER after thapsigargin treatment (Fig. 1 G), and these cells were also resistant to the toxicity of thapsigargin (Fig. S1 K).

Together, these data demonstrate that ER Ca<sup>2+</sup> overload in VMP1-deficient T cells not only causes UPR and ER stress in ER, the organelle where VMP1 resides, but also results in secondary Ca<sup>2+</sup> overload in mitochondria, which is associated with increase of apoptosis. Mitochondrial Ca<sup>2+</sup> overload is an established trigger of cell death (Giorgi et al., 2012). We thus tried to rescue the apoptosis of VMP1-deficient T cells by blocking mitochondrial Ca<sup>2+</sup> uptake. Mitochondrial calcium uniporter (MCU) is important for mitochondrial Ca<sup>2+</sup> uptake at mitochondria-associated membrane (Patergnani et al., 2011), and we found that treatment with the MCU inhibitor Benzethonium (BZN) in vitro reduced mitochondrial Ca<sup>2+</sup> levels in VMP1-deficient T cells (Fig. 5 F), demonstrating mitochondrial Ca<sup>2+</sup> overload causes apoptosis of VMP1-deficient T cells. Finally, we tried to rescue T cell number in *Cd4<sup>Cre</sup>Vmp1<sup>fl/fl</sup>* mice with daily injection of BZN for 4 wk. However, no rescue of T cell number was observed (data not shown). Multiple limitations could explain the failure of in vivo rescue experiments with BZN, including drug dose, duration, and toxicity of BZN itself



**Figure 5. ER  $Ca^{2+}$  overload in VMP1-deficient T cells results in ER stress and secondary  $Ca^{2+}$  overload in mitochondria.** (A) Immunoblot analysis of pelf2 $\alpha$ -S51, eIF2 $\alpha$ , and VMP1 in total T cells freshly isolated from mice with indicated genotypes. Each lane represents an individual mouse. (B) Mitochondrial  $Ca^{2+}$  in T cells from mice with indicated genotypes was examined by flow cytometry with Rhod2. (C) CD4 T cells from mice with indicated genotypes were treated with DMSO or thapsigargin (TG; 1 nM) for 1 h. Mitochondrial  $Ca^{2+}$  was measured by flow cytometry with Rhod2. (D) CD4 T cells from mice with indicated genotypes were treated with DMSO or indicated concentrations of TG for 6 h; apoptosis was measured by flow cytometry. (E) CD4 T cells from mice with indicated genotypes were treated with DMSO or BZN (1  $\mu$ M) for 1 h and mitochondrial  $Ca^{2+}$  was measured by flow cytometry with Rhod2. (F) CD4 T cells from mice with indicated genotypes were treated with DMSO or BZN (1  $\mu$ M) for 6 h; apoptosis was measured by flow cytometry. (G) A model of VMP1 prevention of  $Ca^{2+}$  overload in ER and mitochondria. The balanced activities of VMP1 and SERCA determine the basal level of ER  $Ca^{2+}$  in T cells under steady state. In VMP1-deficient T cells,  $Ca^{2+}$  overload causes ER stress and secondary  $Ca^{2+}$  overload in mitochondria via MCU, which induces cell death.



(A) Representative blots and statistics from one of two independent experiments. (B, C, and E) Representative plots and statistics of Rhod2 mean fluorescence intensity from one of two independent experiments. (D and F) Representative plots and statistics from one of three independent experiments.  $n = 3$  mice per genotype in A, B, D, and E,  $n = 4$  mice per genotype in C and F; each symbol represents an individual mouse; data represent mean  $\pm$  SEM, one-way ANOVA in A–C and E, two-way ANOVA in F; \*\*  $<0.01$ , \*\*\*\*  $<0.001$ . Source data are available for this figure: SourceData F5.

(Fig. 5 F; Patergnani et al., 2011). Taken together, these data demonstrate that ER  $\text{Ca}^{2+}$  overload in VMP1-deficient T cells results in secondary  $\text{Ca}^{2+}$  overload in mitochondria, which causes apoptosis of these cells at least in vitro.

In summary, our data uncover an unexpected but essential role of VMP1-mediated ER  $\text{Ca}^{2+}$  release in maintaining naive T cell survival and immunity. The massive death of VMP1-deficient naive T cells is not related to SOCE because mice with combined deletion of *Stim1/Stim2* or *Orai1/Orai2*, both completely abolishing SOCE in T cells, do not show survival defect of conventional T cells (Oh-Hora et al., 2013; Oh-Hora et al., 2008; Vaeth et al., 2017). Similarly, patients with loss-of-function mutations of STIM1 or ORAI1 have normal T cell numbers (Vaeth and Feske, 2018), demonstrating that SOCE is dispensable for naive T cell survival in human and mice. We propose ER  $\text{Ca}^{2+}$  overload is the origin of phenotypes we observed in VMP1-deficient naive T cells (Fig. 5 G). First, ER  $\text{Ca}^{2+}$  overload induces ER stress (Gwack et al., 2008; Oh-Hora et al., 2008; Vig et al., 2008). Second, ER  $\text{Ca}^{2+}$  overload leads to secondary  $\text{Ca}^{2+}$  overload in mitochondria, a well-known trigger of cell death (Giorgi et al., 2012). Thus, the functions of two key organelles in cells, namely ER and mitochondria, are both affected by VMP1 deficiency, which collectively lead to the death of VMP1-deficient T cells. Future studies with single-channel electrophysiology of VMP1 reconstituted on liposome and/or structural analysis are required to demonstrate whether VMP1 is a  $\text{Ca}^{2+}$  channel or not.

Except for regulating ER  $\text{Ca}^{2+}$  release reported here, VMP1 also regulates autophagy (Ropolo et al., 2007; Zhao et al., 2017) and possesses lipid scramblase activity (Ghanbarpour et al., 2021; Li et al., 2021), both of which could potentially contribute to the phenotypes of VMP1-deficient T cells. However, all T cell phenotypes examined in this study are indistinguishable between *Cd4<sup>Cre</sup>Vmp1<sup>fl/fl</sup>* and *Cd4<sup>Cre</sup>Vmp1<sup>fl/D272N</sup>* mice, demonstrating that a single amino acid responsible for ER  $\text{Ca}^{2+}$  release activity of VMP1 is required for all functions of this protein in T cells and other molecular and cellular defects of VMP1-deficient T cells are likely downstream of or in parallel with ER  $\text{Ca}^{2+}$  overload. Supporting this, our extensive intercrossing of *Vmp1<sup>fl/D272N</sup>* mice did not yield any live pup with *Vmp1<sup>D272N/D272N</sup>* genotype, indicating that like *Vmp1* germline-KO mice (which die around embryonic day 8.5; Calvo-Garrido et al., 2008; Morishita et al., 2019), *Vmp1<sup>D272N/D272N</sup>* mice also have severe developmental defects. Aspartic acid 272 is located within the VMP1, TMEM41, and Tvp38/TMEM64 domain of VMP1, a SNARE-associated domain (Morita et al., 2018), thus we could not exclude the possibility that VMP1 may regulate ER  $\text{Ca}^{2+}$  through interaction with other proteins. VMP1 has been reported to promote SERCA activity in mouse embryonic fibroblasts, although ER  $\text{Ca}^{2+}$  was not measured (Zhao et al., 2017). However, ER  $\text{Ca}^{2+}$  should be decreased rather than increased in VMP1-deficient cells if VMP1 promotes SERCA activity, which

pumps  $\text{Ca}^{2+}$  into ER. It is likely that the decreased SERCA activity observed in that study is a feedback inhibition of SERCA due to ER  $\text{Ca}^{2+}$  overload in VMP1-deficient cells.

ER  $\text{Ca}^{2+}$  homeostasis and ER stress response are associated with many human diseases (Mekahli et al., 2011; Oakes and Papa, 2015; Schrank et al., 2020). Aberrant expression of VMP1 is associated with inflammation (Duseti et al., 2002; Jiang et al., 2004) and cancer (Loncle et al., 2016; Sauermann et al., 2008). VMP1 is also involved in viral infection including SARS-CoV-2 (Hoffmann et al., 2021). Interestingly, SARS-CoV-2 spike protein induces  $\text{Ca}^{2+}$  oscillations that are critical for its infection of cells (Braga et al., 2021). Considering the essential role of VMP1 in maintaining ER  $\text{Ca}^{2+}$  homeostasis and the critical role of ER in viral replication, it is possible that VMP1 regulates viral infection through modulation of ER  $\text{Ca}^{2+}$ . Thus, targeting VMP1 may lead to novel therapies for diseases associated with ER  $\text{Ca}^{2+}$  dysregulation.

## Materials and methods

### Mice

*Vmp1* flox mice and *Vmp1<sup>D272N/+</sup>* mice were generated by services provided by Cyagen Biosciences using CRISPR-assisted gene targeting strategies. To generate *Vmp1* flox allele, the guide RNAs (gRNAs) to mouse *Vmp1* gene (gRNA1: 5'-TTGAATCCAAGTACA ACTACTGG-3', gRNA2: 5'-GACATAAAACCTCTCAATCTAGG-3'; Fig. S3 A), the donor vector containing loxp sites, and Cas9 mRNA were coinjected into fertilized mouse eggs to generate targeted conditional KO offspring. F0 founder animals were identified by PCR followed by sequence analysis, which were bred to C57BL/6J mice to test germline transmission and F1 animal generation. To generate *Vmp1<sup>D272N/+</sup>* allele, the gRNA to mouse *Vmp1* gene (5'-AACCCCTGTTTGACCTGGCTGG-3'), the donor vector containing D272N (GAC to AAT) mutation, and Cas9 mRNA were coinjected into fertilized mouse eggs to generate targeted knockin offspring. F0 founder animals were identified by PCR followed by sequence analysis, which were bred to C57BL/6J mice to test germline transmission and F1 animal generation. *Cd4<sup>Cre</sup>* and 2D2 transgenic were C57BL/6J background and originally from Jackson Laboratory. Age- and sex-matched littermates were used as control in all experiments. Mice were housed under specific pathogen-free conditions at the Laboratory Animal Research Center of Tsinghua University (Beijing, China). The facility was approved by the Beijing Administration Office of Laboratory Animal. All animal works were approved by the Institutional Animal Care and Use Committee of Tsinghua University.

### Cells

HEK293T cells (CRL-11268) and Jurkat cells (TIB-152) were from ATCC. HEK293T cells were maintained in DMEM (Gibco)

supplemented with 5% FBS (Gemini), 2 mM glutamine, 100 U/ml of penicillin, and 100 µg/ml of streptomycin at 37°C in a humidified incubator. Jurkat cells were maintained in RPMI 1640 (Gibco) with the same supplements mentioned above. All cell lines were tested for mycoplasma by the TransDect PCR Mycoplasma detection Kit (TRAN, FM311) and were confirmed to be negative.

Mouse primary T cells were cultured in RPMI1640 medium (Gibco) supplemented with 5% FBS, 2 mM glutamine, 55 µM β-mercaptoethanol, 1 mM sodium pyruvate, 100 U/ml penicillin, 100 µg/ml streptomycin, and 2 ng/ml IL-2 at 37°C in a humidified incubator.

### Antibodies

We used the following antibodies from Cell Signaling Technology: rabbit monoclonal anti-TMEM49/VMP1 (clone D1Y3E), rabbit monoclonal anti-STIM1 (clone D88E10), rabbit monoclonal anti-phospho-eIF2α (Ser51; clone D9G8), and rabbit monoclonal anti-eIF2α (clone D7D3). The following antibodies were obtained from Abcam: recombinant anti-α COPI/COPA (clone EPRI4273[B]) and rabbit polyclonal anti-βCOP (ab2899). The following antibodies were obtained from BioLegend: anti-human PD-1, APC anti-mouse CD4 (GK1.5), APC/Cyanine7 anti-mouse TCRβ (H57-597), PE anti-mouse CD8α (53-6.7), Brilliant Violet 785 anti-mouse CD45.1 (A20), APC anti-mouse CD45.2 (104), and PE anti-mouse IFNγ (XMG1.2). PerCP-Cyanine5.5 anti-Hu/Mo CD44 (IM7) and goat anti-mouse IgG Alexa Fluor Plus 488 were obtained from Invitrogen. eFluor 450 anti-mouse CD8α (53-6.7) was obtained from eBioscience. Mouse monoclonal anti-FLAG (DYKDDDDK) was obtained from Sigma-Aldrich. Mouse monoclonal anti-β-actin was obtained from Santa Cruz.

### CRISPR screening in Jurkat cells

The human genome-wide CRISPR KO pooled library Brunello (#73179; Addgene) was used for the genome-wide KO of genes in Jurkat cells. Lentivirus was produced in HEK293T cells by cotransfection of the Brunello library with psPAX2 and pMD2.G with Chemifect according to the manufacturer's protocol. Virus harvested at 24, 48, and 72 h after transfection were pooled, filtered through 0.45-µm filters, and stored at -80°C as aliquots.

For screening, 80 million Jurkat cells were spin-infected at the multiplicity of infection of 0.5, which gave a coverage of >500 cells/gRNA. After puromycin selection for 3 d and expansion for another 3 d, 1 billion gene-modified Jurkat cells were treated with 10 nM thapsigargin for 48 h at a density of 1 million cells/ml. At the end of thapsigargin treatment, cells were stained with anti-human PD-1 antibody, followed by anti-mouse IgG-Alexa Fluor488 secondary antibody. Dead cells were excluded by LIVE/DEAD Fixable Near-IR dye. Cells with PD-1 expression at the lowest 1% were sorted by a S3e cell sorter (Bio-Rad).

### Genomic DNA (gDNA) extraction for deep sequencing and data analysis

gDNA was extracted by TIANamp Genomic DNA Kit according to manufacturer's protocol. The single guide RNA (sgRNA) sequence from gDNA was amplified with barcoded primers, and amplified PCR products were pooled and followed by gel

purification. The purified products were sequenced with Illumina NovaSeq 6000.

The raw data of next-generation sequencing were deconvoluted with ENCoRE software. The average reads of sgRNA in each sample were between 200 and 500, which were normalized within each sample as reads per million reads to offset the differences in sequencing depth among samples. For each gene, a P value was calculated by paired *t* test for the differences of gRNA abundance between input and end point for four gRNAs.

### CRISPR KO of genes in Jurkat and HEK293T cells

sgRNAs were cloned into LentiCRISPRv2 to knock out specific gene in HEK293T and Jurkat cells. Lentivirus was produced in HEK293T cells by cotransfection of LentiCRISPRv2-sgRNA plasmids targeting specific gene and psPAX2 and pMD2.G by Chemifect according to the manufacturer's protocol. For transduction, 3 million HEK293T or Jurkat cells were suspended in 1 ml fresh medium with 2 ml lentivirus and 8 µg/ml polybrene in 12-well plate, followed by 2,000 *g* centrifugation at 33°C for 2 h, and then the plate was returned to incubator. After 6 h of incubation, cells were detached and transferred to 10-cm dish with fresh medium. 24 h after infection, puromycin (3 µg/ml) was added to cells for selection. Cells were selected for 3 d and expanded for another 3 d before experiments.

To generate monoclonal KO cell lines, HEK293T cells were transiently transfected with LentiCRISPRv2 plasmids targeting specific gene and selected with 3 µg/ml puromycin for 72 h. Then, cells were plated in 96-well plates with approximately one cell per well in DMEM with 15% FBS. After 10 d, single clones were expanded and verified by immunoblot.

### Measurement of Ca<sup>2+</sup> with Fluo4/Fura Red in HEK293T and Jurkat T cells by flow cytometry

Fura Red and Fluo4 were used for Ca<sup>2+</sup> measurement. In all Ca<sup>2+</sup> assays, cells were plated at same density in 6-well plates 1 d before experiment to exclude the influence of cell density. 1 million control or gene-modified HEK293T or Jurkat were resuspended in 250 µl Ca<sup>2+</sup> assay medium (DMEM for HEK293T, RPMI 1640 for Jurkat and primary T cells, and both mediums were supplemented with 25 mM Hepes [pH = 7.4] and 2.5% FBS). Fura Red and Fluo4 were mixed and prepared as 2× solution in 250 µl Ca<sup>2+</sup> assay medium. Then, the 250 µl medium with cells and 250 µl medium with 2× Fura Red and Fluo4 mixture were mixed together, and the final concentration of both Fura Red and Fluo4 was 2 µM. The mixtures were incubated at 37°C for 30 min in the dark. Cells were washed once with Ca<sup>2+</sup> assay medium and resuspended in 800 µl Ca<sup>2+</sup> assay medium for flow cytometry analysis.

For measurement of thapsigargin-induced Ca<sup>2+</sup> influx directly, we placed cell suspension on the cytometer, adjusted the baseline intensities for Fluo4 (FITC channel) and Fura Red (PerCP-Cy5.5 channel), and recorded for 60 s. Then we removed the tube from the cytometer (without stopping the acquisition/recording) and quickly added thapsigargin to a final concentration of 10 nM or 1 µM as indicated. Samples were quickly mixed and returned to the cytometer. The total assay time was indicated in each experiment.

For measurement of ER  $\text{Ca}^{2+}$  and SOCE, cell suspension was supplemented with 2 mM final concentration of EGTA before being placed on cytometer. The concentration of  $\text{Ca}^{2+}$  is 0.42 mM in RPMI 1640 and 1.8 mM in DMEM, so 2 mM EGTA can completely chelate the extracellular  $\text{Ca}^{2+}$ . We adjusted the baseline intensities for Fluo4 (FITC channel) and Fura Red (PerCP-Cy5.5 channel) and recorded for 60 s. Then we removed the tube from the cytometer and quickly added thapsigargin to a final concentration of 1  $\mu\text{M}$ . Samples were quickly mixed, returned to the cytometer, and recorded for another 420 s. Then, we removed the tube from the cytometer (without stopping the acquisition/recording) and quickly added  $\text{CaCl}_2$  to a final concentration of 2 mM (the  $\text{Ca}^{2+}$  in the assay medium was not included in this 2 mM concentration). Samples were quickly mixed, returned to the cytometer, and recorded for another 420 s. All measurements were performed at 25°C.

For measurement of  $\text{Ca}^{2+}$  influx in cells transfected with plasma membrane-targeted VMP1, dye-loaded cells were recorded for 60 s. Then we removed the tube from the cytometer (without stopping the acquisition/recording) and quickly added 8 mM or indicated concentration of  $\text{CaCl}_2$ . Samples were quickly mixed, returned to the cytometer, and recorded for another 240 s.

#### Measurement of $\text{Ca}^{2+}$ sensors RCaMP1h and G-CEPIA1er by flow cytometry

The cDNAs of G-CEPIA1er and RCaMP1h were obtained by gene synthesis (Sangon) and cloned into a lentiviral vector pLJM1. Cell line stably expressing sensors were established by lentiviral transduction. Then, VMP1 was knocked out in this cell line by methods described above. For measurement of the fluorescence of RCaMP1h or G-CEPIA1er, 1 million cells were suspended in 800  $\mu\text{l}$   $\text{Ca}^{2+}$  assay medium. We placed cell suspension on the cytometer and G-CEPIA1er (GFP channel) was recorded for 60 s. Then we removed the tube from cytometer and quickly added thapsigargin to a final concentration of 1  $\mu\text{M}$ . Samples were quickly mixed, returned to the cytometer, and recorded for another 840 s. The total assay time for each sample was 900 s. The voltages for GFP (for G-CEPIA1er)/PE (RCaMP1h) channels were kept unchanged for all samples. In overexpression studies, sensor cells were transfected with indicated constructs with a BFP reporter and the influence of overexpression on the intensity of the sensor was measured on BFP-high cells.

#### Overexpression experiments

The full-length cDNA of human VMP1 was cloned into two different systems for overexpression. To overexpress proteins at high levels, we used a small vector pCMV with a backbone of 3.7 kb. This vector does not contain fluorescent marker, so a pCMV-BFP construct was cotransfected to gate out BFP-high cells for analysis on flow cytometry. For moderate expression in rescue experiments, we used a lentiviral vector called pLJM1-BFP, which was a modified pLJM1 vector whose puromycin cassette was replaced by BFP. This moderate overexpression system was used in rescue experiments in Figs. 4 and S3. In all other experiments, pCMV-based overexpression system was used.

#### Immunofluorescence

HEK293T cells were plated on poly-d-lysine Cellware 12-mm coverslips (BD Biosciences). On the next day, cells were transfected with indicated plasmids. 24 h after transfection, cells were rinsed once with PBS, stained with WGA for 10 min at 37°C (WGA: Invitrogen, Cat: W32466), washed twice with PBS, and then fixed for 15 min with 4% paraformaldehyde in PBS at room temperature. Cells were rinsed twice with PBS and permeabilized by methanol (prechilled at -20°C) for 10 min on ice. After rinsing three times with PBS, the slides were blocked by 5% BSA for 30 min at room temperature and incubated with primary antibodies (diluted 1:500 in 5% BSA) for 1–3 h at room temperature, rinsed four times with PBS, and incubated with goat-anti-mouse Alexa Fluor secondary antibodies (diluted 1:1,000 in 5% BSA) for 1 h at room temperature in the dark. Slides were washed four times with PBS, mounted on glass coverslips using ProLong Gold (Invitrogen) with DAPI, and imaged on a Zeiss780 confocal microscope with a 63 $\times$  oil lens.

#### Screening of VMP1 inhibitor

To examine whether  $\text{Ca}^{2+}$  influx induced by VMP1-K404/406A can be inhibited by compounds targeting known membrane transporters/ion channels, we tested a collection of 652 membrane transporter/ion channel related compounds (HY-L011A from MCE; the information of the library is available in Table S2). HEK293T-RcaMP1h cells were transfected with pCMV-VMP1-K404/406A together with a BFP reporter. 24 h after transfection, cells were preincubated with each compound individually at the concentration of 20  $\mu\text{M}$  for 30 min and then  $\text{Ca}^{2+}$  influx in BFP<sup>high</sup> cells was measured by flow cytometry with 8 mM  $\text{CaCl}_2$ . DMSO and EGTA (10 mM) were used as controls.

#### Western blot

After treatment as indicated, cells were collected and washed with cold PBS. Cells were lysed with lysis buffer (1% Triton X-100, 40 mM Hepes [pH 7.4], 10 mM  $\beta$ -glycerol phosphate, 10 mM pyrophosphate) supplemented with EDTA-free protease inhibitor cocktail (Thermo Fisher Scientific) on ice for 15 min. The soluble fractions of cell lysates were isolated by centrifugation at 14,000 rpm for 6 min. Proteins were denatured by the addition of 6 $\times$  SDS sampling buffer and boiling for 5 min at 95°C. Samples were subjected to SDS-PAGE and immunoblot analysis.

#### Electrophysiology

STIM1-KO HEK293T cells were used for whole-cell patch-clamp recording. Cells were plated on poly-d-lysine coated 25-mm coverslips one day before transfection. pCMV-GFP and pCMV-VMP1-K404/406A were co-transfected to select the positive cells under a fluorescence microscope. pCMV-GFP transfection alone was used as negative control. 6 h after transfection, the culture medium was replaced by calcium-free DMEM (Thermo Fisher Scientific) to avoid toxicity of sustained  $\text{Ca}^{2+}$  influx induced by VMP1-K404/406A. Whole-cell patch-clamp recordings were performed 18–24 h after transfection.

The coverslip with transfected cells was transferred into a recording chamber, the recording bath solution includes: 150 mM

NaCl, 10 mM TEA-Cl, 2 mM MgCl<sub>2</sub>, 10 mM Hepes, and 30 mM glucose with pH adjusted to 7.4. The cells were imaged under an inverted microscope and an iXon EMCCD camera controlled by Andor SOLIS software; GFP-positive cells were selected for recording. Borosilicate glass pipettes (B15014F) were made with a pipette puller (PC-10, NARISHIGE) to resistances of 3–5 MΩ. Intracellular pipette solution includes 120 mM CsCl, 3 mM MgCl<sub>2</sub>, 10 mM EGTA, 10 mM Hepes, and 8 mM NaCl with pH adjusted to 7.3. All recordings were performed at room temperature. The sampling rate was 5 kHz and the voltage clamp used a -100 mV holding potential. The data were acquired using a patch-clamp amplifier (SUTTER IPA/E-100157) and controlled by Igor Pro software.

#### L. monocytogenes infection

For primary infection, 5,000 CFUs of *L. monocytogenes* expressing the chicken ovalbumin were injected into mice via tail vein. On day 8 after infection, mice were sacrificed and splenocytes were isolated to measure antigen-specific CD8 T cell response by flow cytometry. Briefly, splenocytes were stained with CD8α-PB, TCRβ-APC, CD44-PerCP-Cy5.5, and PE-conjugated H-2Kb-OVA<sup>257-264</sup> tetramer for 30 min at 37°C. Cells were washed twice with FACS buffer and analyzed on a BD flow cytometer. Dead cells were excluded by DAPI staining. Splenocytes were also stimulated with OVA<sup>257-264</sup> peptide (SIINFEKL) for 5 h ex vivo in the presence of monensin for examination of INFγ production by flow cytometry.

#### BM transplantation

Total BM cells from congenically marked competitor mice (CD45.1) and *Cd4<sup>Cre</sup>Vmp1<sup>fl/fl</sup>* mice (CD45.2) were mixed at 1:1 ratio and transferred into lethally irradiated (4.5 Gy, twice with 2 h apart) recipient mice (CD45.1/2) via tail vein. Mice were maintained in water with antibiotics for the first 2 wk and then on normal water. Chimerism of B cells and T cells in spleen of recipient mice were examined 8 wk after transplantation.

#### Flow cytometry analysis of primary T cell phenotypes

Single-cell suspensions were prepared from thymi, spleens, and lymph nodes by grinding through 70-μm strainer. Erythrocytes were depleted by hypotonic lysis. For staining of surface markers, cells were incubated in FACS buffer (PBS supplemented with 1% calf serum, 1% penicillin/streptomycin, and 2 mM EDTA) with indicated combinations of antibodies for 15 min at 4°C and Fc blockade (2G4) to prevent non-specific binding. Cells were washed twice with FACS buffer and DAPI was included to exclude dead cells.

For apoptosis assays, T cells were stained with surface marker, then Annexin V staining was performed following the instructions of Annexin V-FITC Apop Kit. Samples were recorded with an LSR Fortessa cytometer (BD) and analyzed with FlowJo software (BD).

For caspase-3 staining assay, T cells were incubated with 10 μM FITC-C6-DEVD-FMK (Cat: 13408; AAT Bioquest) in Hank's buffer containing 20 mM Hepes for 1 h at 37°C. Surface marker staining was performed following the incubation of FITC-C6-DEVD-FMK. Samples were recorded with an LSR Fortessa cytometer (BD) and analyzed with FlowJo software (BD).

For measurement of mitochondrial membrane potential of WT and VMP1-deficient T cells, primary T cells from lymph nodes were incubated with 2 μM TMRM (tetramethylrhodamine, methyl ester) dye (Cat: HY-D0984A; MCE) in RPMI 1640 for 1 h at 37°C. Then cells were washed to remove TMRM dye and stained with surface marker for 10 min at room temperature. Samples were recorded with an LSR Fortessa cytometer (BD) and analyzed with FlowJo software (BD).

For measurement of ER Ca<sup>2+</sup> stored in primary T cells, single-cell suspensions were loaded with Fluo4/Fura Red dye and antibodies for Fc blockade, B220-PB, CD4-APC, and CD8-PE in RPMI 1640 with 5 mM EGTA for 30 min at 37°C. Cells were washed once with RPMI 1640 with 5 mM EGTA and resuspended in RPMI 1640 with 5 mM EGTA. We placed cell suspension on the cytometer, adjusted the baseline intensities for Fluo4 (FITC channel) and Fura Red (PerCP-Cy5.5 channel) with B220<sup>+</sup> cells (from control mice) as the reference, and recorded for 60 s. Then we removed the tube from the cytometer (without stopping the acquisition/recording) and quickly added 1 μM of ionomycin (final concentration) as indicated. Samples were quickly mixed, returned to the cytometer, and recorded for another 240 s. All samples were recorded with the exact same parameters.

For measurement of mitochondrial Ca<sup>2+</sup>, we used serum-free RPMI 1640 with 5 mM EGTA as assay buffer to minimize the influences of growth factors and extracellular Ca<sup>2+</sup> on mitochondrial Ca<sup>2+</sup>. Cells were washed once with RPMI 1640 with 5 mM EGTA and then incubated with 1 μM of Rhod2-AM and antibodies for Fc blockade, CD4-APC, and CD8-PB in RPMI 1640 with 5 mM EGTA at 37°C for 30 min. Cells were washed twice and resuspended in RPMI 1640 medium with 5 mM EGTA. DAPI was used to exclude dead cells. Samples were acquired with an LSR Fortessa cytometer (BD).

#### MCU inhibitor treatment

Single-cell suspensions prepared from control or *Cd4<sup>Cre</sup>Vmp1<sup>fl/fl</sup>* mice were pretreated with DMSO or 1 μM of benzethonium chloride in RPMI 1640 with 5 mM EGTA for 1 h at 37°C. Then, cells were incubated with mitochondrial Ca<sup>2+</sup> dye Rhod2 (1 μM) and Fc blockade, CD4-APC, and CD8-PB in RPMI 1640 with 5 mM EGTA for 30 min at 37°C in the presence of DMSO or 1 μM benzethonium chloride. After incubation, cells were washed twice with RPMI 1640 with 5 mM EGTA and mitochondrial Ca<sup>2+</sup> was measured as mentioned above.

For examination of the effect of benzethonium chloride on T cell apoptosis, cells were treated with DMSO or 1 μM benzethonium chloride in RPMI 1640 for 6 h at 37°C. Then, apoptosis was measured as described above.

#### Thapsigargin treatment

Single-cell suspensions prepared from control or *Cd4<sup>Cre</sup>Vmp1<sup>fl/fl</sup>* mice were resuspended in RPMI 1640 with 5 mM EGTA. This calcium-free medium was used for the whole experiment to avoid SOCE induced by thapsigargin, which activates T cells and influences the measurement of mitochondrial Ca<sup>2+</sup> by Rhod2. Cells were treated with DMSO or 1 nM thapsigargin in RPMI 1640 with 5 mM EGTA for 1 h at 37°C and then mitochondrial Ca<sup>2+</sup> was measured as described above. Thapsigargin (1 nM) was

present in the whole experiment. For apoptosis assays, cells were treated with DMSO, 1, 10, or 100 nM of thapsigargin in RPMI 1640 for 6 h at 37°C, and then apoptosis was measured as described above.

### Statistics and reproducibility

GraphPad Prism 8.0 was used for statistical analysis. Data are presented as individual values or mean  $\pm$  SEM as indicated in figure legends. The P values and number of replicates (*n*) are shown in figures or figure legends. A two-tailed unpaired Student's *t* test was used to evaluate the difference between two groups. *P* < 0.05 was considered significant. All experiments were repeated independently at least twice with similar results. Representative flow plots, immunoblots, and micrographs were selected from biological replicates.

### Online supplemental material

**Fig. S1** validates the effect of TG on PD-1 expression and survival of Jurkat T cells. It also shows the KO efficiency of VMP1 protein in HEK293T cells, as well as the effect of VMP1 deficiency on ER Ca<sup>2+</sup>, SOCE, and response to the toxicity of TG in HEK293T cells. **Fig. S2** shows the induction of Ca<sup>2+</sup> influx by plasma membrane-targeted VMP1-K404/406A in HEK293T cells and the roles of STIM1 and ORAI1 in such Ca<sup>2+</sup> influx. It also shows the effect of inhibitors targeting known channels/pores on Ca<sup>2+</sup> influx induced by plasma membrane-targeted VMP1-K404/406A in HEK293T cells. **Fig. S3** shows the generation and characterization of *Cd4<sup>Cre</sup>Vmp1<sup>fl/fl</sup>* mice and *Cd4<sup>Cre</sup>Vmp1<sup>fl/D272N</sup>* mice. It also shows the system used to express endogenous level of VMP1, as well as the relationship between ER Ca<sup>2+</sup> regulation and VMP1's other functions. Table S1 shows the results of CRISPR screening of PD-1 modulators in Jurkat T cells. Table S2 shows the information of compounds in HY-L011A library from MCE.

### Data availability

All data from this study have been shown in figures and supplementary materials.

### Acknowledgments

We thank H. Qi's lab, Y. Shi's lab, and B. Xiao's lab for help with calcium assays. We thank Institute for Immunology at Tsinghua University for providing and maintaining equipment.

This research was supported by National Natural Science Foundation of China (grant 31741085 to M. Peng and 31800747 to N. Yin), Tsinghua University Initiative Scientific Research Program (to M. Peng), and funds from Tsinghua-Peking Center for Life Sciences and Institute for Immunology at Tsinghua University (to M. Peng).

Author contributions: Y. Liu, Y. Ma, J. Xu, G. Zhang, and X. Zhao designed and performed experiments and analyzed data. Z. He and L. Wang performed experiments. N. Yin analyzed data and supervised the project. M. Peng conceived, designed, and supervised the project, analyzed data, and wrote the paper with input from all authors.

Disclosures: The authors declare no competing interests exist.

Submitted: 21 June 2022

Revised: 11 January 2023

Accepted: 10 March 2023

### References

- Akerboom, J., N. Carreras Calderón, L. Tian, S. Wabnig, M. Prigge, J. Toló, A. Gordus, M.B. Orger, K.E. Severi, J.J. Macklin, et al. 2013. Genetically encoded calcium indicators for multi-color neural activity imaging and combination with optogenetics. *Front. Mol. Neurosci.* 6:2. <https://doi.org/10.3389/fnmol.2013.00002>
- Alberts, B., A. Johnson, J. Lewis, M. Raff, K. Roberts, and P. Walter. 2002. *Molecular Biology of the Cell*. Fourth edition. Garland Science, New York.
- Arakel, E.C., and B. Schwappach. 2018. Correction: Formation of COPI-coated vesicles at a glance (doi:10.1242/jcs.209890). *J. Cell Sci.* 131:jcs218347. <https://doi.org/10.1242/jcs.218347>
- Berridge, M.J., P. Lipp, and M.D. Bootman. 2000. The versatility and universality of calcium signalling. *Nat. Rev. Mol. Cell Biol.* 1:11–21. <https://doi.org/10.1038/35036035>
- Bird, G.S., W.I. DeHaven, J.T. Smyth, and J.W. Putney Jr. 2008. Methods for studying store-operated calcium entry. *Methods.* 46:204–212. <https://doi.org/10.1016/j.ymeth.2008.09.009>
- Bootman, M.D., and G. Bultynck. 2020. Fundamentals of cellular calcium signaling: A primer. *Cold Spring Harb. Perspect. Biol.* 12:12. <https://doi.org/10.1101/cshperspect.a038802>
- Braga, L., H. Ali, I. Secco, E. Chiavacci, G. Neves, D. Goldhill, R. Penn, J.M. Jimenez-Guardeño, A.M. Ortega-Prieto, R. Bussani, et al. 2021. Drugs that inhibit TMEM16 proteins block SARS-CoV-2 spike-induced syncytia. *Nature.* 594:88–93. <https://doi.org/10.1038/s41586-021-03491-6>
- Calvo-Garrido, J., S. Carilla-Latorre, F. Lázaro-Diéguez, G. Egea, and R. Escalante. 2008. Vacuole membrane protein 1 is an endoplasmic reticulum protein required for organelle biogenesis, protein secretion, and development. *Mol. Biol. Cell.* 19:3442–3453. <https://doi.org/10.1091/mbc.e08-01-0075>
- Camello, C., R. Lomax, O.H. Petersen, and A.V. Tepikin. 2002. Calcium leak from intracellular stores--the enigma of calcium signalling. *Cell Calcium.* 32:355–361. <https://doi.org/10.1016/S0143416002001926>
- De Mario, A., A. Tosatto, J.M. Hill, J. Kriston-Vizi, R. Ketteler, D. Vecellio Reane, G. Cortopassi, G. Szabadkai, R. Rizzuto, and C. Mammucari. 2021. Identification and functional validation of FDA-approved positive and negative modulators of the mitochondrial calcium uniporter. *Cell Rep.* 35:109275. <https://doi.org/10.1016/j.celrep.2021.109275>
- Duseti, N.J., Y. Jiang, M.I. Vaccaro, R. Tomasini, A. Azizi Samir, E.L. Calvo, A. Ropolo, F. Fiedler, G.V. Mallo, J.C. Dagorn, and J.L. Iovanna. 2002. Cloning and expression of the rat vacuole membrane protein 1 (VMP1), a new gene activated in pancreas with acute pancreatitis, which promotes vacuole formation. *Biochem. Biophys. Res. Commun.* 290:641–649. <https://doi.org/10.1006/bbrc.2001.6244>
- Ghanbarpour, A., D.P. Valverde, T.J. Melia, and K.M. Reinisch. 2021. A model for a partnership of lipid transfer proteins and scramblases in membrane expansion and organelle biogenesis. *Proc. Natl. Acad. Sci. USA.* 118:e2101562118. <https://doi.org/10.1073/pnas.2101562118>
- Giorgi, C., F. Baldassari, A. Bononi, M. Bonora, E. De Marchi, S. Marchi, S. Missiroli, S. Patergnani, A. Rimessi, J.M. Suski, et al. 2012. Mitochondrial Ca(2+) and apoptosis. *Cell Calcium.* 52:36–43. <https://doi.org/10.1016/j.ceca.2012.02.008>
- Giunti, R., A. Gamberucci, R. Fulceri, G. Bánhegyi, and A. Benedetti. 2007. Both translocon and a cation channel are involved in the passive Ca<sup>2+</sup> leak from the endoplasmic reticulum: A mechanistic study on rat liver microsomes. *Arch. Biochem. Biophys.* 462:115–121. <https://doi.org/10.1016/j.abb.2007.03.039>
- Gwack, Y., S. Srikanth, M. Oh-Hora, P.G. Hogan, E.D. Lamperti, M. Yamashita, C. Gelinas, D.S. Neems, Y. Sasaki, S. Feske, et al. 2008. Hair loss and defective T- and B-cell function in mice lacking ORAI1. *Mol. Cell Biol.* 28:5209–5222. <https://doi.org/10.1128/MCB.00360-08>
- Hoffmann, H.H., W.M. Schneider, K. Rozen-Gagnon, L.A. Miles, F. Schuster, B. Razoosky, E. Jacobson, X. Wu, S. Yi, C.M. Rudin, et al. 2021. TMEM41B is a pan-flavivirus host factor. *Cell.* 184:133–148.e20. <https://doi.org/10.1016/j.cell.2020.12.005>
- Hogan, P.G., R.S. Lewis, and A. Rao. 2010. Molecular basis of calcium signaling in lymphocytes: STIM and ORAI. *Annu. Rev. Immunol.* 28:491–533. <https://doi.org/10.1146/annurev.immunol.021908.132550>

- Jiang, P.H., Y. Motoo, M.I. Vaccaro, J.L. Iovanna, G. Okada, and N. Sawabu. 2004. Expression of vacuole membrane protein 1 (VMP1) in spontaneous chronic pancreatitis in the WBN/Kob rat. *Pancreas*. 29:225–230. <https://doi.org/10.1097/O0006676-200410000-00008>
- Lewis, R.S. 2011. Store-operated calcium channels: New perspectives on mechanism and function. *Cold Spring Harb. Perspect. Biol.* 3:a003970. <https://doi.org/10.1101/cshperspect.a003970>
- Li, Y.E., Y. Wang, X. Du, T. Zhang, H.Y. Mak, S.E. Hancock, H. McEwen, E. Pandzic, R.M. Whan, Y.C. Aw, et al. 2021. TMEM41B and VMP1 are scramblases and regulate the distribution of cholesterol and phosphatidylserine. *J. Cell Biol.* 220:220. <https://doi.org/10.1083/jcb.202103105>
- Lomax, R.B., C. Camello, F. Van Coppenolle, O.H. Petersen, and A.V. Tepikin. 2002. Basal and physiological Ca<sup>2+</sup> leak from the endoplasmic reticulum of pancreatic acinar cells. Second messenger-activated channels and translocons. *J. Biol. Chem.* 277:26479–26485. <https://doi.org/10.1074/jbc.M201845200>
- Loncle, C., M.I. Molejon, S. Lac, J.I. Tellechea, G. Lomberk, L. Gramatica, M.F. Fernandez Zapico, N. Dusetti, R. Urrutia, and J.L. Iovanna. 2016. The pancreatitis-associated protein VMP1, a key regulator of inducible autophagy, promotes Kras(G12D)-mediated pancreatic cancer initiation. *Cell Death Dis.* 7:e2295. <https://doi.org/10.1038/cddis.2016.202>
- Martonosi, A., and R. Feretos. 1964. Sarcoplasmic reticulum. I. the uptake of Ca<sup>++</sup> by sarcoplasmic reticulum fragments. *J. Biol. Chem.* 239:648–658. [https://doi.org/10.1016/S0021-9258\(18\)51731-2](https://doi.org/10.1016/S0021-9258(18)51731-2)
- Mekahli, D., G. Bultynck, J.B. Parys, H. De Smedt, and L. Missiaen. 2011. Endoplasmic-reticulum calcium depletion and disease. *Cold Spring Harb. Perspect. Biol.* 3:3. <https://doi.org/10.1101/cshperspect.a004317>
- Morishita, H., Y.G. Zhao, N. Tamura, T. Nishimura, Y. Kanda, Y. Sakamaki, M. Okazaki, D. Li, and N. Mizushima. 2019. A critical role of VMP1 in lipoprotein secretion. *Elife*. 8:e48834. <https://doi.org/10.7554/eLife.48834>
- Morita, K., Y. Hama, T. Izume, N. Tamura, T. Ueno, Y. Yamashita, Y. Sakamaki, K. Mimura, H. Morishita, W. Shihoya, et al. 2018. Genome-wide CRISPR screen identifies TMEM41B as a gene required for autophagosome formation. *J. Cell Biol.* 217:3817–3828. <https://doi.org/10.1083/jcb.201804132>
- Oakes, S.A., and F.R. Papa. 2015. The role of endoplasmic reticulum stress in human pathology. *Annu. Rev. Pathol.* 10:173–194. <https://doi.org/10.1146/annurev-pathol-012513-104649>
- Oestreich, K.J., H. Yoon, R. Ahmed, and J.M. Boss. 2008. NFATc1 regulates PD-1 expression upon T cell activation. *J. Immunol.* 181:4832–4839. <https://doi.org/10.4049/jimmunol.181.7.4832>
- Oh-Hora, M., N. Komatsu, M. Pishyareh, S. Feske, S. Hori, M. Taniguchi, A. Rao, and H. Takayanagi. 2013. Agonist-selected T cell development requires strong T cell receptor signaling and store-operated calcium entry. *Immunity*. 38:881–895. <https://doi.org/10.1016/j.immuni.2013.02.008>
- Oh-Hora, M., M. Yamashita, P.G. Hogan, S. Sharma, E. Lamperti, W. Chung, M. Prakriya, S. Feske, and A. Rao. 2008. Dual functions for the endoplasmic reticulum calcium sensors STIM1 and STIM2 in T cell activation and tolerance. *Nat. Immunol.* 9:432–443. <https://doi.org/10.1038/nri1574>
- Owsianik, G., K. Talavera, T. Voets, and B. Nilius. 2006. Permeation and selectivity of TRP channels. *Annu. Rev. Physiol.* 68:685–717. <https://doi.org/10.1146/annurev.physiol.68.040204.101406>
- Patergnani, S., J.M. Suski, C. Agnoletto, A. Bononi, M. Bonora, E. De Marchi, C. Giorgi, S. Marchi, S. Missiroli, F. Poletti, et al. 2011. Calcium signaling around Mitochondria Associated Membranes (MAMs). Cell communication and signaling. *Cell Commun. Signal.* 9:19. <https://doi.org/10.1186/1478-811X-9-19>
- Prakriya, M., and R.S. Lewis. 2015. Store-operated calcium channels. *Physiol. Rev.* 95:1383–1436. <https://doi.org/10.1152/physrev.00020.2014>
- Ropolo, A., D. Grasso, R. Pardo, M.L. Sacchetti, C. Archange, A. Lo Re, M. Seux, J. Nowak, C.D. Gonzalez, J.L. Iovanna, and M.I. Vaccaro. 2007. The pancreatitis-induced vacuole membrane protein 1 triggers autophagy in mammalian cells. *J. Biol. Chem.* 282:37124–37133. <https://doi.org/10.1074/jbc.M706956200>
- Roy, A., and W.F. Wonderlin. 2003. The permeability of the endoplasmic reticulum is dynamically coupled to protein synthesis. *J. Biol. Chem.* 278:4397–4403. <https://doi.org/10.1074/jbc.M207295200>
- Sammels, E., J.B. Parys, L. Missiaen, H. De Smedt, and G. Bultynck. 2010. Intracellular Ca<sup>2+</sup> storage in health and disease: A dynamic equilibrium. *Cell Calcium.* 47:297–314. <https://doi.org/10.1016/j.ceca.2010.02.001>
- Sauermann, M., O. Sahin, H. Sultmann, F. Hahne, S. Blaszkiewicz, M. Majety, K. Zatloukal, L. Füzesi, A. Poustka, S. Wiemann, and D. Arlt. 2008. Reduced expression of vacuole membrane protein 1 affects the invasion capacity of tumor cells. *Oncogene*. 27:1320–1326. <https://doi.org/10.1038/sj.onc.1210743>
- Schrank, S., N. Barrington, and G.E. Stutzmann. 2020. Calcium-handling defects and neurodegenerative disease. *Cold Spring Harb. Perspect. Biol.* 12:12. <https://doi.org/10.1101/cshperspect.a035212>
- Suzuki, J., K. Kanemaru, K. Ishii, M. Ohkura, Y. Okubo, and M. Iino. 2014. Imaging intraorganellar Ca<sup>2+</sup> at subcellular resolution using CEPIA. *Nat. Commun.* 5:4153. <https://doi.org/10.1038/ncomms5153>
- Tábara, L.C., and R. Escalante. 2016. VMP1 establishes ER-microdomains that regulate membrane contact sites and autophagy. *PLoS One*. 11:e0166499. <https://doi.org/10.1371/journal.pone.0166499>
- Thastrup, O., P.J. Cullen, B.K. Drøbak, M.R. Hanley, and A.P. Dawson. 1990. Thapsigargin, a tumor promoter, discharges intracellular Ca<sup>2+</sup> stores by specific inhibition of the endoplasmic reticulum Ca<sup>2+</sup>(+)-ATPase. *Proc. Natl. Acad. Sci. USA*. 87:2466–2470. <https://doi.org/10.1073/pnas.87.7.2466>
- Treback, M., and J.P. Kinet. 2019. Calcium signalling in T cells. *Nat. Rev. Immunol.* 19:154–169. <https://doi.org/10.1038/s41577-018-0110-7>
- Vaeth, M., and S. Feske. 2018. Ion channelopathies of the immune system. *Curr. Opin. Immunol.* 52:39–50. <https://doi.org/10.1016/j.coi.2018.03.021>
- Vaeth, M., S. Kahlfuss, and S. Feske. 2020. CRAC channels and calcium signaling in T cell-mediated immunity. *Trends Immunol.* 41:878–901. <https://doi.org/10.1016/j.it.2020.06.012>
- Vaeth, M., J. Yang, M. Yamashita, I. Zee, M. Eckstein, C. Knosp, U. Kaufmann, P. Karoly Jani, R.S. Lacruz, V. Flockerzi, et al. 2017. ORAI2 modulates store-operated calcium entry and T cell-mediated immunity. *Nat. Commun.* 8:14714. <https://doi.org/10.1038/ncomms14714>
- Vig, M., W.I. DeHaven, G.S. Bird, J.M. Billingsley, H. Wang, P.E. Rao, A.B. Hutchings, M.H. Jouvin, J.W. Putney, and J.P. Kinet. 2008. Defective mast cell effector functions in mice lacking the CRACM1 pore subunit of store-operated calcium release-activated calcium channels. *Nat. Immunol.* 9:89–96. <https://doi.org/10.1038/nri1550>
- Wang, W.A., L.B. Agellon, and M. Michalak. 2019. Organellar calcium handling in the cellular reticular network. *Cold Spring Harb. Perspect. Biol.* 11:11. <https://doi.org/10.1101/cshperspect.a038265>
- Wuytack, F., L. Raeymaekers, and L. Missiaen. 2002. Molecular physiology of the SERCA and SPCA pumps. *Cell Calcium.* 32:279–305. <https://doi.org/10.1016/S0143416002001847>
- Xu, C., B. Bailly-Maitre, and J.C. Reed. 2005. Endoplasmic reticulum stress: Cell life and death decisions. *J. Clin. Invest.* 115:2656–2664. <https://doi.org/10.1172/JCI26373>
- Zhao, Y.G., Y. Chen, G. Miao, H. Zhao, W. Qu, D. Li, Z. Wang, N. Liu, L. Li, S. Chen, et al. 2017. The ER-localized transmembrane protein EPG-3/VMP1 regulates SERCA activity to control ER-isolation membrane contacts for autophagosome formation. *Mol. Cell.* 67:974–989.e6. <https://doi.org/10.1016/j.molcel.2017.08.005>

## Supplemental material

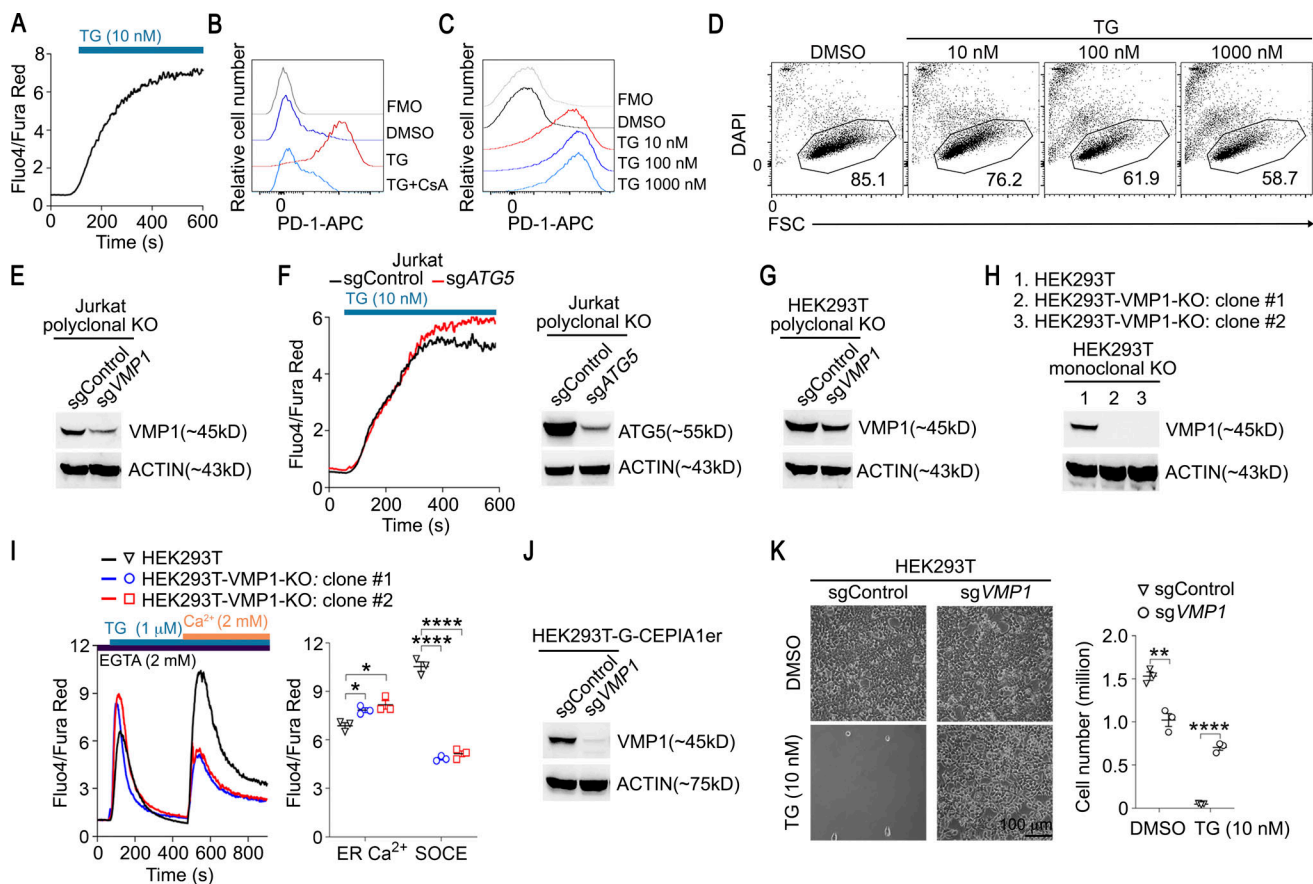


Figure S1. **Additional supporting data related to Fig. 1.** (A) SOCE in thapsigargin (TG)-treated Jurkat cells was measured by flow cytometry. (B) Jurkat cells were treated with DMSO, TG (10 nM), or TG (10 nM) plus CsA (1 μM) for 48 h. The expression of PD-1 was examined by flow cytometry. Mean fluorescence intensities of PD-1 staining are shown; FMO is unstained control. (C) Jurkat cells were treated with DMSO or indicated concentrations of TG for 48 h. PD-1 expression was examined. Mean fluorescence intensities of PD-1 staining are shown; FMO is unstained control. (D) Jurkat cells were treated as in C. The percentage of live cells was determined by flow cytometry with DAPI staining. (E) The expression of VMP1 in Jurkat cells expressing indicated sgRNAs and Cas9 was analyzed by immunoblot. (F) TG-induced Ca<sup>2+</sup> influx in Jurkat cells expressing indicated sgRNA and Cas9 was examined by flow cytometry, and the expression of ATG5 was analyzed by immunoblot. (G) The expression of VMP1 in HEK293T cells expressing indicated sgRNAs, and Cas9 was analyzed by immunoblot. (H) Validation of monoclonal VMP1-KO HEK293T cells by immunoblot. (I) ER Ca<sup>2+</sup> and SOCE in VMP1-KO cells were examined by flow cytometry. (J) The expression of VMP1 in HEK293T-G-CEPIA1er cells expressing indicated sgRNAs and Cas9 was analyzed by immunoblot. (K) 1 × 10<sup>5</sup> HEK293T cells expressing indicated sgRNAs and Cas9 were plated in 12-well plates. 24 h later, cells were treated with DMSO or TG (10 nM) for another 48 h. (A–D and F) Representative plots from one of three independent experiments. (E–H and J) Representative blots from one of two independent experiments. (I and K) Representative plots and statistics from one of three independent experiments. *n* = 3 in I and K. Each symbol represents one sample; data represent mean ± SEM, one-way ANOVA in I, two-tailed unpaired *t* test in K; \* <0.05, \*\* <0.01, \*\*\* <0.001. Source data are available for this figure: SourceData FS1.

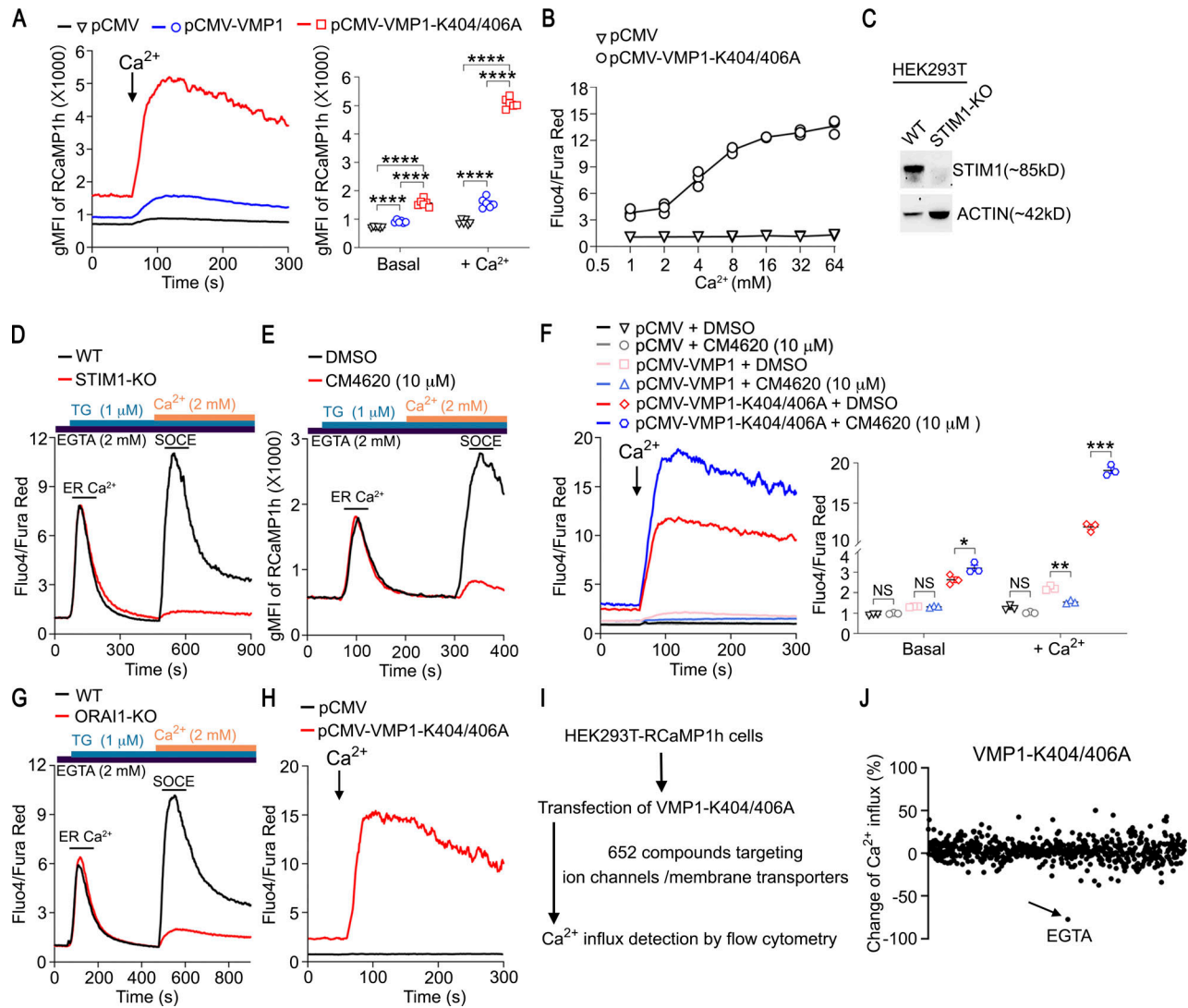


Figure S2. **Additional supporting data related to Fig. 2.** (A) Ca<sup>2+</sup> influx in HEK293T-RCaMP1h cells transfected with empty vector, VMP1, or VMP1-K404/406A was measured by flow cytometry with 8 mM CaCl<sub>2</sub>. (B) Ca<sup>2+</sup> influx in HEK293T cells transfected with empty vector or VMP1-K404/406A was measured by flow cytometry with Fluo4/Fura Red at indicated concentrations of CaCl<sub>2</sub>. (C) The expression of STIM1 in WT and STIM1-KO HEK293T cells was examined by immunoblot. (D) ER Ca<sup>2+</sup> and SOCE in WT and STIM1-KO HEK293T cells were measured by flow cytometry. (E) HEK293T-RCaMP1h cells were preincubated with DMSO or CM4620 for 30 min. ER Ca<sup>2+</sup> and SOCE were measured by flow cytometry. (F) HEK293T cells were transfected with indicated plasmids. Cells were preincubated with DMSO or CM4620 for 30 min, then Ca<sup>2+</sup> influx was measured by flow cytometry with 8 mM CaCl<sub>2</sub>. (G) ER Ca<sup>2+</sup> and SOCE in WT and ORAI1-KO HEK293T cells were measured by flow cytometry. (H) ORAI1-KO HEK293T cells were transfected with indicated plasmids; Ca<sup>2+</sup> influx was measured by flow cytometry with 8 mM CaCl<sub>2</sub>. (I) Strategy for screening of potential VMP1 inhibitor from a compound library targeting known ion channels/membrane transporters (HY-L011A from MCE; the information of library is available in Table S2). (J) HEK293T-RCaMP1h cells were transfected with pCMV-VMP1-K404/406A together with a BFP reporter. 24 h after transfection, cells were preincubated with each compound individually at the concentration of 20 μM for 30 min, then Ca<sup>2+</sup> influx in BFP-high cells was measured by flow cytometry with 8 mM CaCl<sub>2</sub>. A summary of screening result is shown. EGTA was used as a positive control. (A and F) Representative plots and statistics from one of three independent experiments. (B, D, E, G, and H) Representative plots from one of three independent experiments. (C) Representative blots from one of two independent experiments. *n* = 5 in A, *n* = 3 in F; each symbol represents one sample; data represent mean ± SEM, two-way ANOVA in A and F; \* <0.05, \*\* <0.01, \*\*\* <0.001, \*\*\*\* <0.0001. Source data are available for this figure: SourceData FS2.



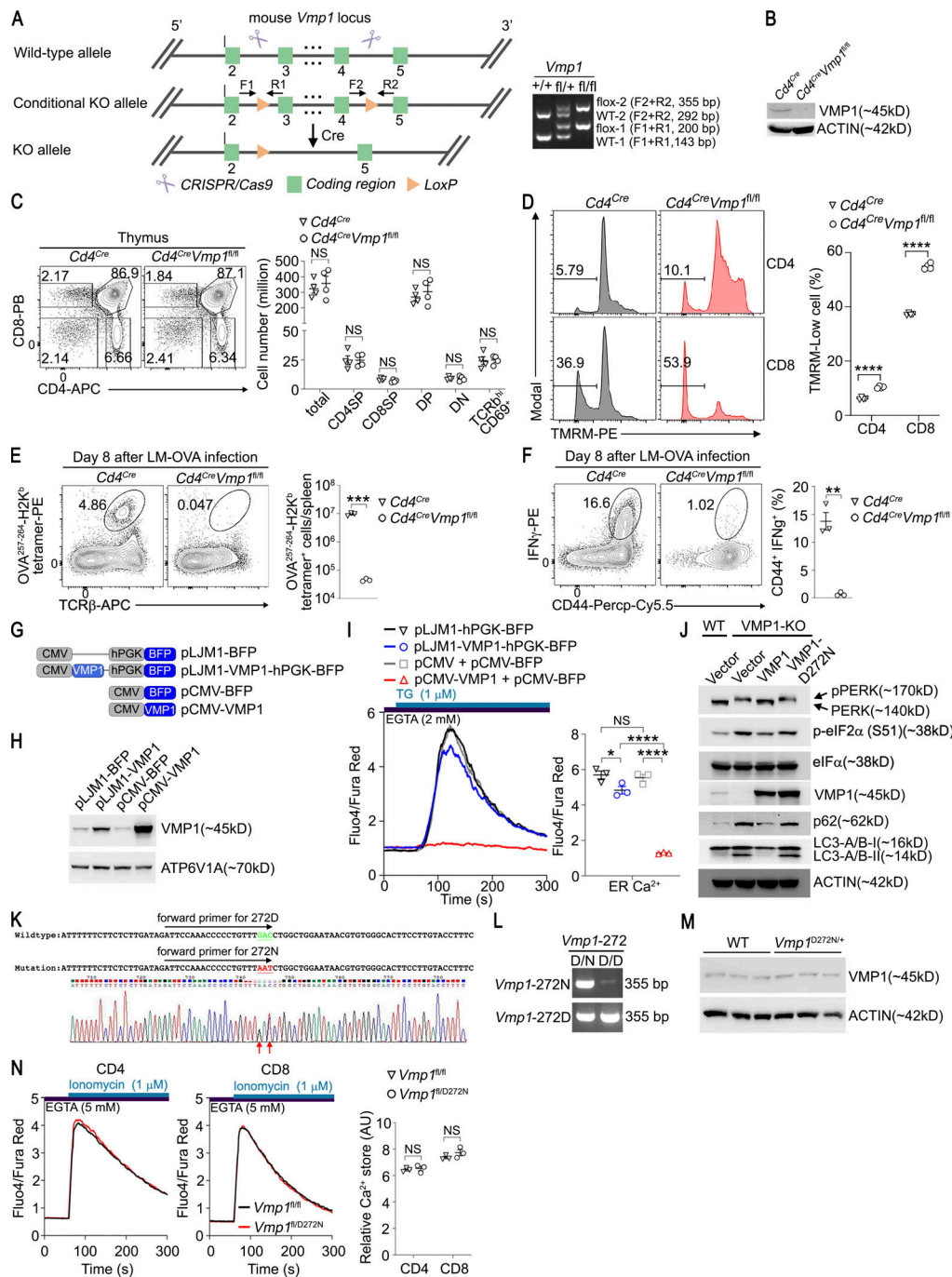


Figure S3. **Additional supporting data related to Figs. 3 and 4.** (A) Gene targeting strategy and genotyping of tail DNA from mice with indicated genotypes. (B) Immunoblot analysis of VMP1 expression in T cells from mice with indicated genotypes. (C) Thymi from mice with indicated genotypes were analyzed by flow cytometry. (D) TMRM level in T cells from mice with indicated genotypes was examined by flow cytometry. (E and F) Mice with indicated genotypes were infected with *L. monocytogenes* expressing OVA (LM-OVA). CD8 T cell response was analyzed on day 8 after infection. (E) Representative plots and statistics of OVA<sup>257-264</sup>-H2K<sup>b</sup> tetramer-positive cells in spleen are shown. Plots were gated on single live cells. (F) Representative plots and statistics of IFN $\gamma$ -positive cells after ex vivo stimulation with OVA<sup>257-264</sup> peptide (SIINFEKL) are shown. Plots were gated on CD8 $\alpha$ <sup>+</sup> cells. (G) pLJM1- or pCMV-based expression system. (H) HEK293T cells were transfected with indicated plasmids, and the expression of VMP1 was examined by immunoblot. (I) ER Ca<sup>2+</sup> in HEK293T cells transfected with indicated plasmids was measured by flow cytometry. (J) The expression of indicated proteins in HEK293T cells or VMP1-KO HEK293T cells stably expressing empty vector, VMP1, or VMP1-D272N was analyzed by immunoblot. (K) gDNA sequence of *Vmp1* loci from WT and *Vmp1*<sup>D272N/+</sup> mice. Nucleotides encoding 272D (GAC) and 272N (AAT) are labeled with green and red colors, respectively. Arrows indicate double peaks of G/A and C/T reads from sequencing result. (L) PCR genotyping of WT and *Vmp1*<sup>D272N/+</sup> mice. (M) Immunoblot analysis of VMP1 expression in T cells from mice with indicated genotypes. (N) ER Ca<sup>2+</sup> stored in T cells from mice with indicated genotypes was examined by flow cytometry. (B, H, J, and M) Representative blots from one of three independent experiments. (C-F, I, and N) Representative plots and statistics from one of three independent experiments. *n* = 4 mice per genotype in C and D, *n* = 3 mice per genotype in E, F, I, and N; each symbol represents an individual mouse; data represent mean  $\pm$  SEM, two-tailed unpaired *t* test in C-F and N, one-way ANOVA in I; \* < 0.05, \*\* < 0.01, \*\*\* < 0.001, \*\*\*\* < 0.0001. Source data are available for this figure: SourceData FS3.

Provided online are two tables. Table S1 shows the results of CRISPR screening of PD-1 modulators in Jurkat T cells. Table S2 shows the information of compounds in HY-L011A library from MCE.